

2-3 Results of Geophysical Survey

2-3-1 Interpretation Results of Geophysical Survey

Apparent resistivity of each of ten frequencies was calculated at the field. Using such apparent resistivity, apparent resistivity pseudosections for all of 10 survey lines were made, as shown in Figures II-2-12(1) to II-2-12(5). And apparent resistivity plan maps for five frequencies, 1,024 Hz, 512 Hz, 256 Hz, 64 Hz and 16 Hz, were also made, as shown in Figures II-2-13(1) to II-2-13(5).

(1) Pseudosections

The lack of stations are found on the several pseudosections, such as stations 2 and 4 of survey line A. This is due to the exception of stations, at which low quality and low S/N data were obtained because those stations were located in the swamp and/or near the root.

On the pseudosection, horizontal axis corresponds to distance and vertical axis to frequencies.

1) Line-A (Section-A)

This pseudosection was provided using the CSAMT data of stations 1 through 13, with the exception of those of stations 2 and 4.

Apparent resistivities of less than 100 $\Omega\cdot m$ are predominantly distributed, and those of more than 1,000 $\Omega\cdot m$ are locally found.

Between stations 1 and 3, apparent resistivities between 100 $\Omega\cdot m$ and 500 $\Omega\cdot m$ are distributed within the whole frequency range. And between stations 5 and 7 and between 9 and 13, apparent resistivities of more than 100 $\Omega\cdot m$ are dominated within higher-to-middle frequency range, but in lower frequency range, values of apparent resistivities decrease toward the lower frequencies.

Apparent resistivities of more than 1,000 $\Omega\cdot m$ are locally distributed in higher-to-middle frequency range between stations 6 and 7 and between stations 12 and 13.

Apparent resistivities of less than 100 $\Omega\cdot m$ are dominated between stations 8 and 10, at which the existence of the geological boundary and/or the fault structure is suggested.

2) Line-B (section-B)

This pseudosection was provided using the data of stations 16 through 28.

Apparent resistivities show the lateral distribution between stations 19 and 23 and between stations 24 and 28, and the horizontal distribution at the stations 16 through 18. Between

stations 16 and 18, apparent resistivities of more than 150 $\Omega\cdot\text{m}$ are distributed in the whole frequency range, and those at the medium frequency range show higher values than those of higher and lower frequency ranges.

On the other hand, at the stations 19 through 23, apparent resistivities of more than 150 $\Omega\cdot\text{m}$ are distributed at higher frequency range, but within middle-to-lower frequency range those values decrease towards lower frequencies and at lower frequencies of less than 16 Hz those show values of less than 20 $\Omega\cdot\text{m}$. The tendency of this decrease in apparent resistivities towards lower frequency range can be found between stations 24 and 28.

3) Line-C (Section-C)

This pseudosection was provided by using the data of stations 30 through 42.

Different distribution patterns are found at the both sides of station 33.

At the western side of station 33, apparent resistivities of less than 100 $\Omega\cdot\text{m}$ and of more than 400 $\Omega\cdot\text{m}$ are distributed laterally and show a strong apparent resistivity contrast, which suggests the existence of geologic boundary and/or the fault structure. Apparent resistivity zone of less than 100 $\Omega\cdot\text{m}$ may correspond to the fault structure. And apparent resistivity zone of more than 400 $\Omega\cdot\text{m}$ may reflect high resistivity rock/layer.

While, at the eastern side of station 35, apparent resistivities show the horizontal distribution, that is, those of more than 100 $\Omega\cdot\text{m}$ at higher frequency range, and those of less than 50 $\Omega\cdot\text{m}$ at middle-to-lower frequency range.

4) Line-D (Section-D)

This pseudosection was provided by using the data of stations 43 through 55.

This line shows a similar distribution pattern as that in Line-C, in a such manner as that the different distribution patterns are found at the both sides of stations 47.

At the western side of station 47, namely between stations 44 and 46, a lateral distribution pattern of apparent resistivities of more than 250 $\Omega\cdot\text{m}$ is dominated at the whole frequency range. This lateral distribution pattern of apparent resistivities can be seen in each of all lines of the south of the Line-B, so that it is suggested that the resistivity structure causing this lateral distribution pattern extends in N-S direction.

While, at the eastern side of station 47, apparent resistivities show the horizontal distribution, that is, those of more than 100 $\Omega\cdot\text{m}$ are distributed at higher-to-middle frequency range, and those values decrease towards lower frequencies. Those show of less than 10 $\Omega\cdot\text{m}$ at the frequencies of lower than 16 Hz.

Dense iso-apparent resistivity lines of between stations 46 and 47 suggest the existence of the fault structures, extending from the Line-C.

5) Line-E (Section-E)

This pseudosection was provided by using the data of stations 57 through 67.

Notable apparent resistivity variation is found between stations 61 through 63 at the central part, but the both sides show a little variations, suggesting the existence of homogeneous and isotropic layer/rock.

Apparent resistivities of more than 500 $\Omega\cdot\text{m}$ are distributed between stations 59 and 60.

The two low zones of less than 50 $\Omega\cdot\text{m}$ are found vertically at station 61 and at station 63, in a such manner as to divide the distribution of apparent resistivities of more than 100 $\Omega\cdot\text{m}$. These two zones may suggest the existence of fault structures, which may correspond to extension of fault structures found on the Line-D. While the latter fault structure corresponds to the one found at station 51 on Line-D, at which the apparent resistivity contrast is weaker than that in this line.

6) Line-F (Section-F)

This pseudosection was provided by using the CSAMT data of stations 70 through 79.

A similar distribution pattern as that of the Line-E could be observed on this pseudosection. However, apparent resistivities of more than 400 $\Omega\cdot\text{m}$ are distributed in a smaller area than those in the Line-E, and those of less than 100 $\Omega\cdot\text{m}$ show a wider distribution.

Apparent resistivities of more than 400 $\Omega\cdot\text{m}$ are distributed in the whole frequency range at station 72 and in the higher frequency range between stations 78 and 79.

While, apparent resistivities of less than 100 $\Omega\cdot\text{m}$ are widely distributed in the middle-to-lower frequency range at stations 74 through 77, and those values decrease towards the lower frequencies. Those at the frequency of less than 32 Hz are of less than 10 $\Omega\cdot\text{m}$.

7) Line-G (Section-G)

This pseudosection was provided by using the CSAMT data of stations 81 through 91.

A similar distribution pattern as that of the Line-F is observed, suggesting that the resistivity structure below the Line-F extends toward the south.

Apparent resistivities of more than 400 $\Omega\cdot\text{m}$ are distributed at station 84 and between stations 89 and 90. Those at the former become a local distribution, showing a smaller distribution pattern than that in the Line-F. On the other hand, those at the latter, found in the higher

frequency range in the Line-F, are distributed in the medium-to-lower frequency range in this section, suggesting that a layer causing those of more than 400 $\Omega\cdot\text{m}$ become thicker towards the south.

While, apparent resistivities of less than 100 $\Omega\cdot\text{m}$ are dominated at stations 85 through 89, and those values decrease towards the lower frequencies.

Resistivity discontinuity lines, causing strong apparent resistivity contrasts, seem to exist at station 83 and at station 89.

8) Line-H (Section-H)

This pseudosection was provided by using the CSAMT data of stations 93 through 101.

Apparent resistivities show different patterns at the both sides of station 96.

At the west of station 96, apparent resistivities of more than 100 $\Omega\cdot\text{m}$ are predominantly distributed. However, the apparent resistivity zone of more than 400 $\Omega\cdot\text{m}$, observed in each pseudosection of the Lines-A through-G, is found locally at the lower frequency range than 8Hz, and apparent resistivities of the zone become of more than 250 $\Omega\cdot\text{m}$.

On the other hand, at the east of station 96, apparent resistivities of less than 100 $\Omega\cdot\text{m}$ are distributed predominantly in the medium-to-lower frequency range, and decrease those distribution area than those in the Line-G. But those of more than 100 $\Omega\cdot\text{m}$ increase those distribution area in a such manner as to fill the decrement area of those of less than 100 $\Omega\cdot\text{m}$. While, those of less than 100 $\Omega\cdot\text{m}$ are observed at the lower frequency range than 512 Hz at station 93.

9) Line-I (Section-I)

This pseudosection was provided by using the CSAMT data of stations 103 through 112.

Lateral distribution patterns, suggesting the existence of many fault structures, are found on this pseudosection.

Apparent resistivities of less than 100 $\Omega\cdot\text{m}$ are distributed in the whole frequency range at the stations 104 and 111 in a such manner as to divide those of more than 100 $\Omega\cdot\text{m}$, suggesting the existence of fault structures near the both stations.

Those of less than 100 $\Omega\cdot\text{m}$ observed between stations 107 and 109 seem to be due to the same geologic environment at the east of station 97 of the Line-H, which may correspond to the fault structures and/or accompanying fracture zones.

Those of more than 100 $\Omega\cdot\text{m}$ are distributed in the lower frequency range than 32 Hz at station 106, and in the higher frequency range than 512 Hz at stations 110 and 112.

10) Line-J (Section-J)

This pseudosection was provided by using the CSAMT data of stations 113 through 122.

A similar distribution pattern as that on the Line-I is observed. Therefore, it is suggested that the vertical structures are predominantly distributed.

Apparent resistivities of more than $400 \Omega\cdot\text{m}$ is distributed in the whole frequency range at the west of station 114.

Apparent resistivities of less than $100 \Omega\cdot\text{m}$ are widely distributed at the east of station 115. Between stations 115 and 118, although those of more than $100 \Omega\cdot\text{m}$ are found locally in the lower frequency range, those of lower than $100 \Omega\cdot\text{m}$ are observed in the whole frequency range. And those are also found in the frequency range of lower than 64 Hz between stations 118 and 120, and in the whole frequency range at station 121. These low apparent resistivities of less than $100 \Omega\cdot\text{m}$ may reflect mainly the fault structures, taking the N-S trending resistivity structure into consideration.

(2) Plan Maps

Five frequencies, 1,024 Hz, 512 Hz, 256 Hz, 64 Hz and 16 Hz, each of which is thought to be suitable for the interpretation, were adopted, among the ten audio-frequencies, 2,048, 1,024, 512, 256, 128, 64, 32, 16, 8 and 4 Hz. Apparent resistivity plan maps of the above frequencies are shown in the Figures II-2-13(1) to II-2-13(5).

1) 1,024 Hz

A distribution pattern of apparent resistivities shows a trend of N-S direction, reflecting an N-S trending resistivity structure.

Apparent resistivities of more than $400 \Omega\cdot\text{m}$ are distributed at the following three parts:

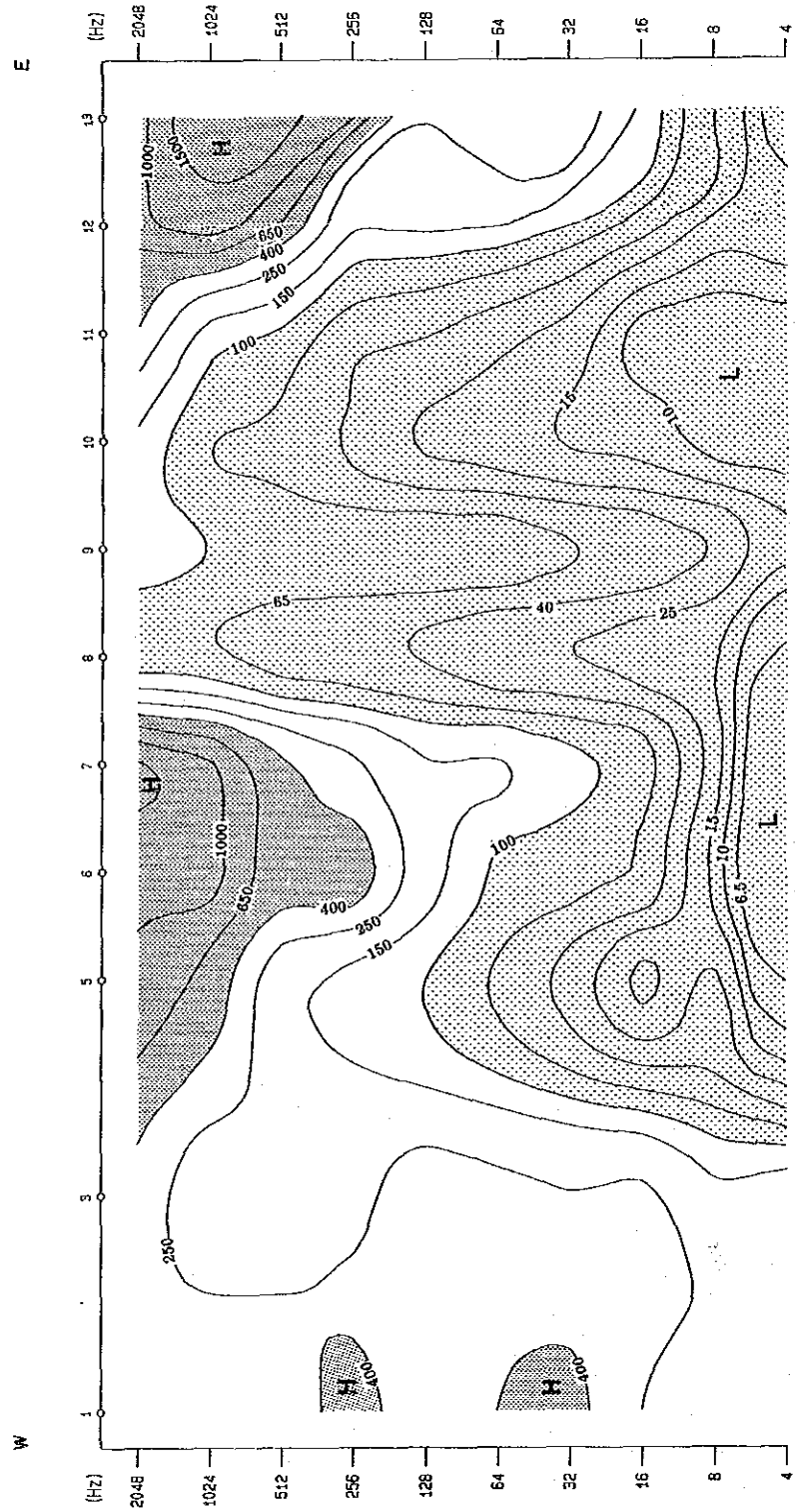
- a) Central part of Line-A at the northern part of the survey area.
- b) Eastern ends of the survey area.
- c) Western part of the survey area.

Among these items, those at the item a) are distributed locally, showing no extension toward the south. A distribution pattern of those at the item b) suggests an extension of the formation causing those toward the east beyond the survey area. And those at the item c) show a distribution width of about 200 m through 250 m in NNW-SSE direction and extend up to the Line-G.

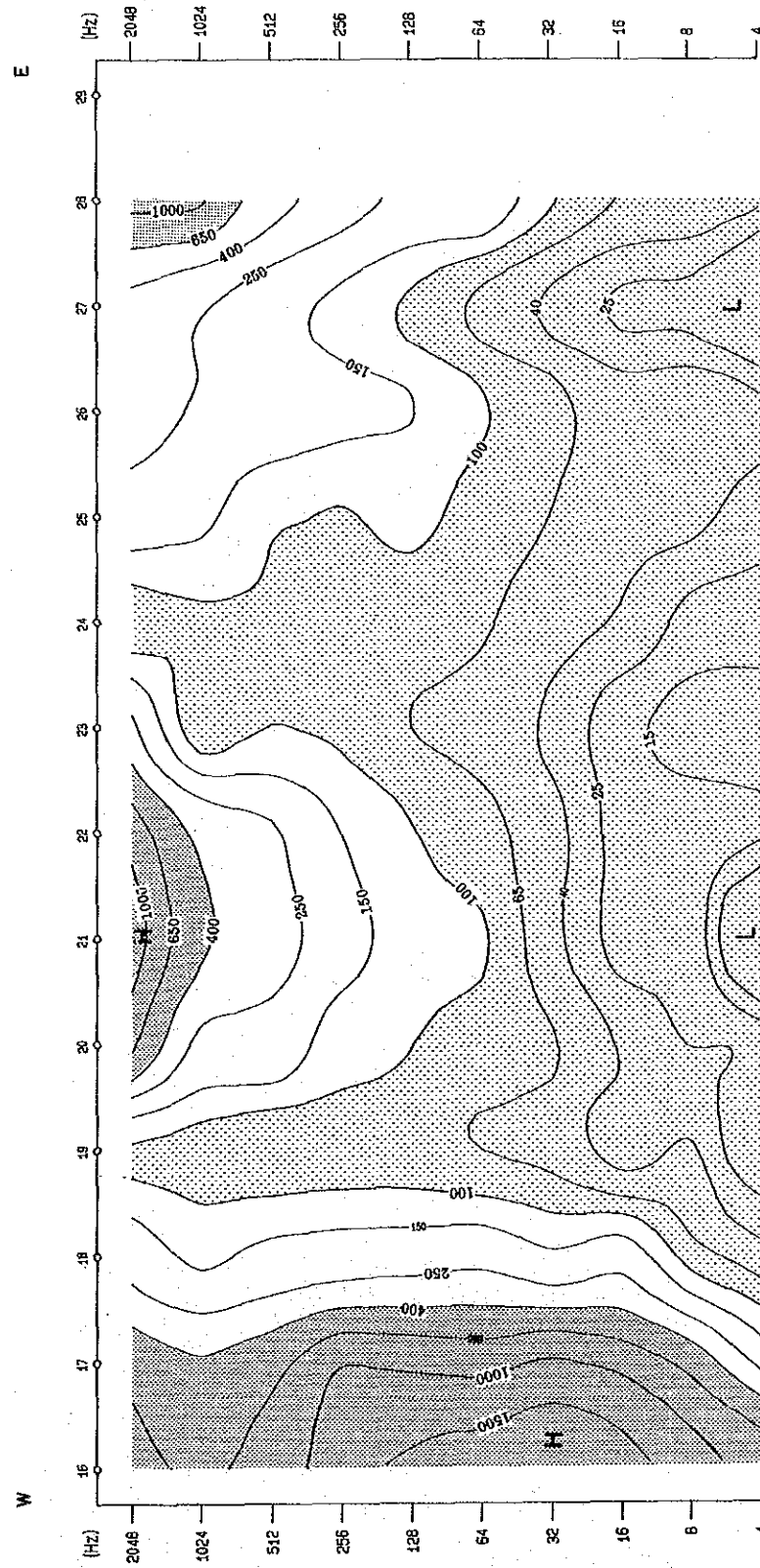
Apparent resistivities of less than $100 \Omega\cdot\text{m}$ are distributed at the following six parts:

- d) Central parts of Lines-A through -J.
- e) Western parts of Lines-B through -E.

Section - A



Section - B

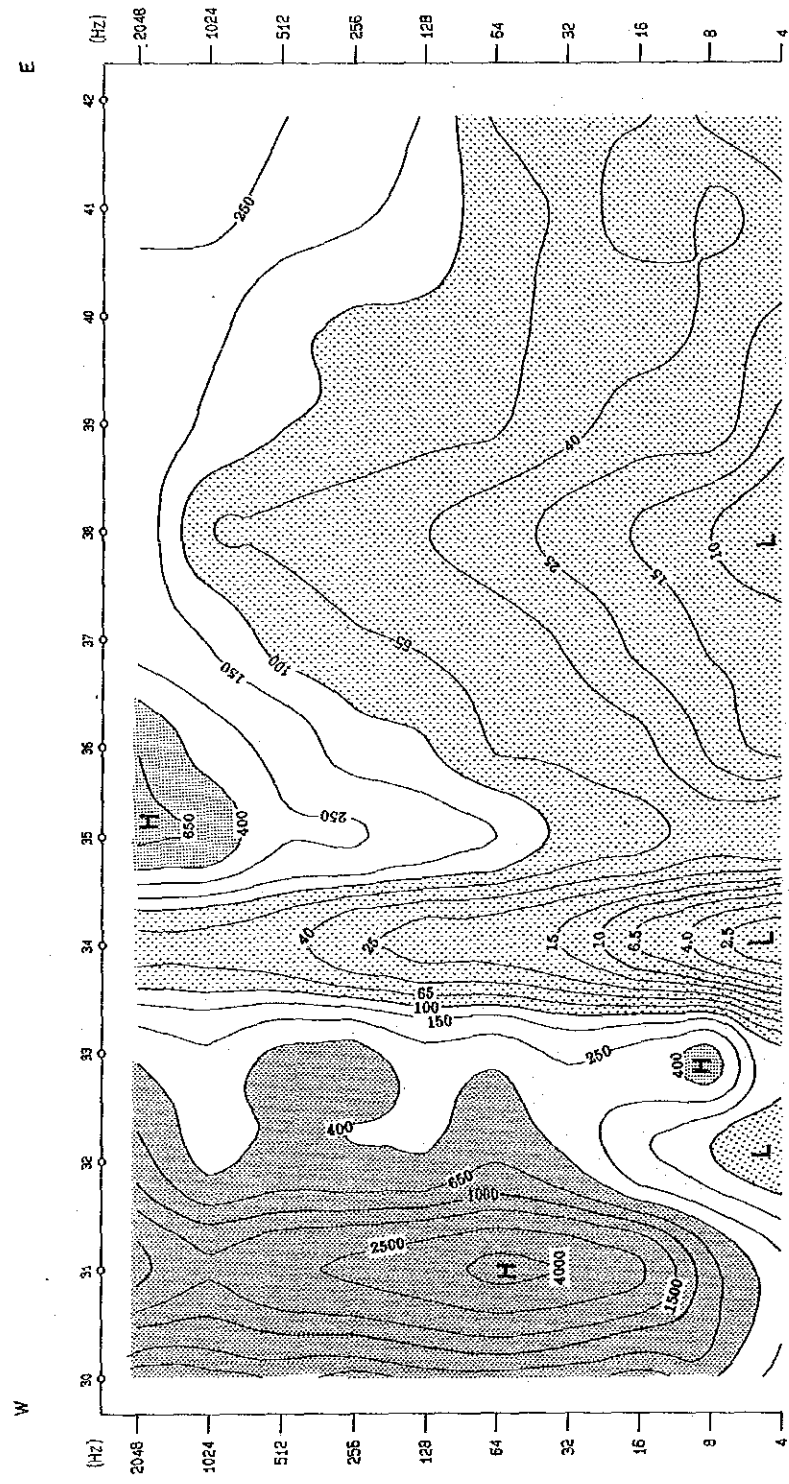


LEGEND

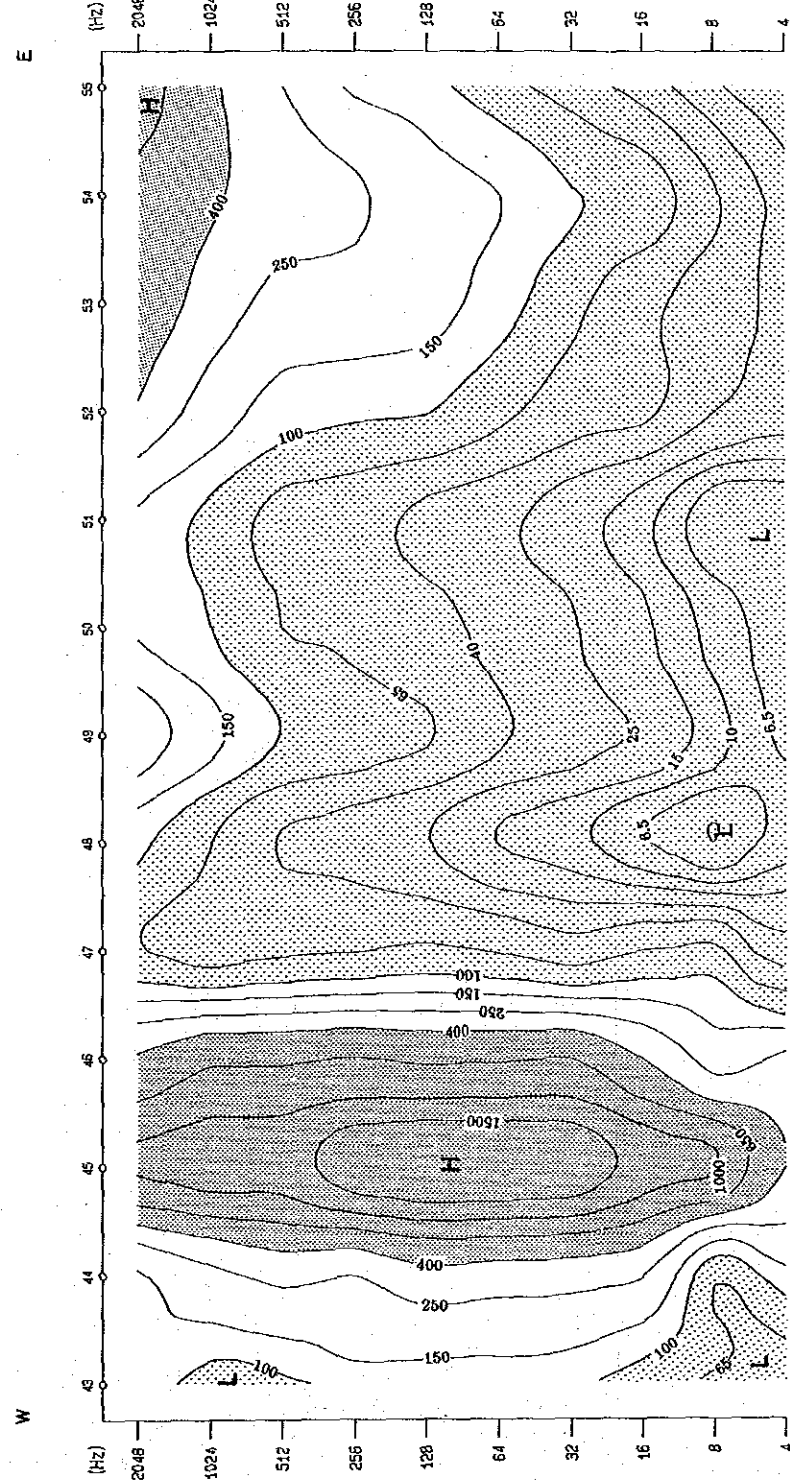
- 100 ○ Station and No.
- Resistivity Contour (Unit: ohm-m.)
- $\rho < 100$ ohm-m
- 400 ohm-m $\leq \rho$
- * ρ : Resistivity

Fig. II-2-12 (1) Apparent Resistivity Section (Section-A, B)

Section - C



Section - D

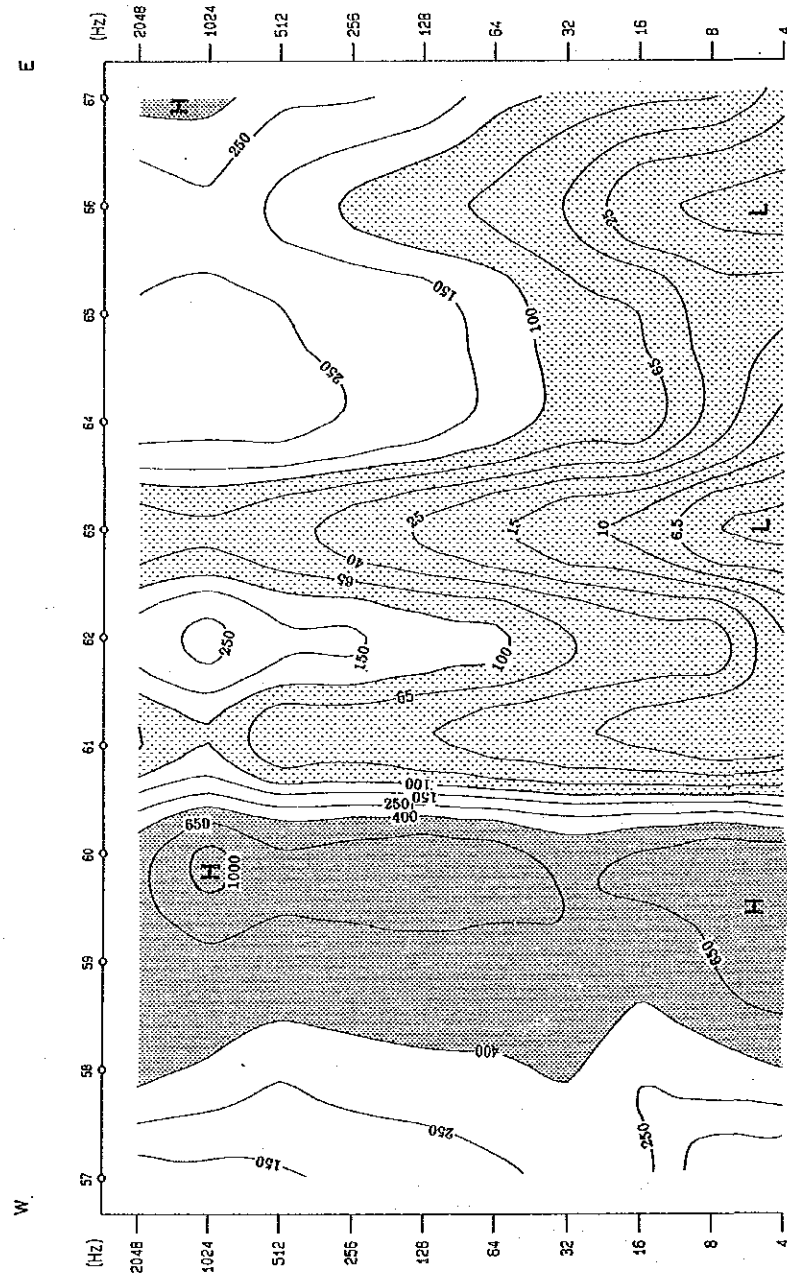


LEGEND

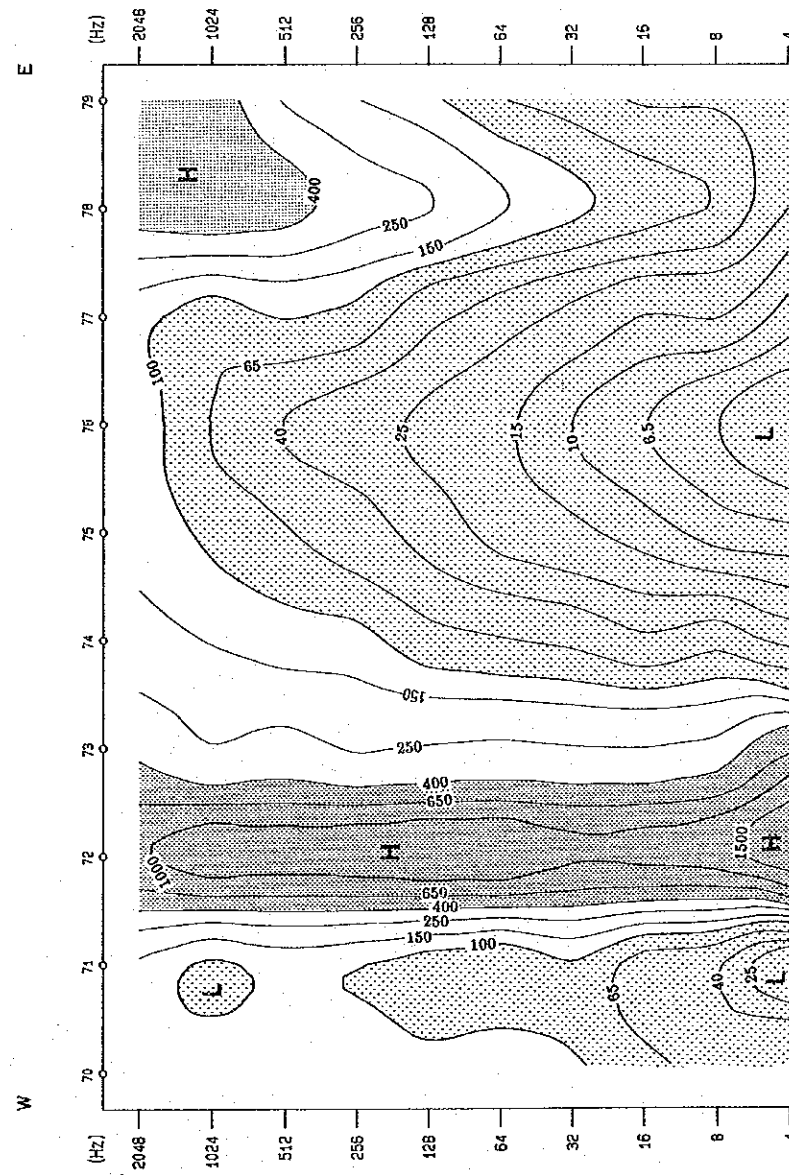
- Station and No. 100 ○
- Resistivity Contour (Unit: ohm-m) 100 250 500
- $\rho < 100$ ohm-m L
- 400 ohm-m $\leq \rho$ H
- * ρ : Resistivity

Fig. II-2-12 (2) Apparent Resistivity Section (Section-C, D)

Section - E



Section - F

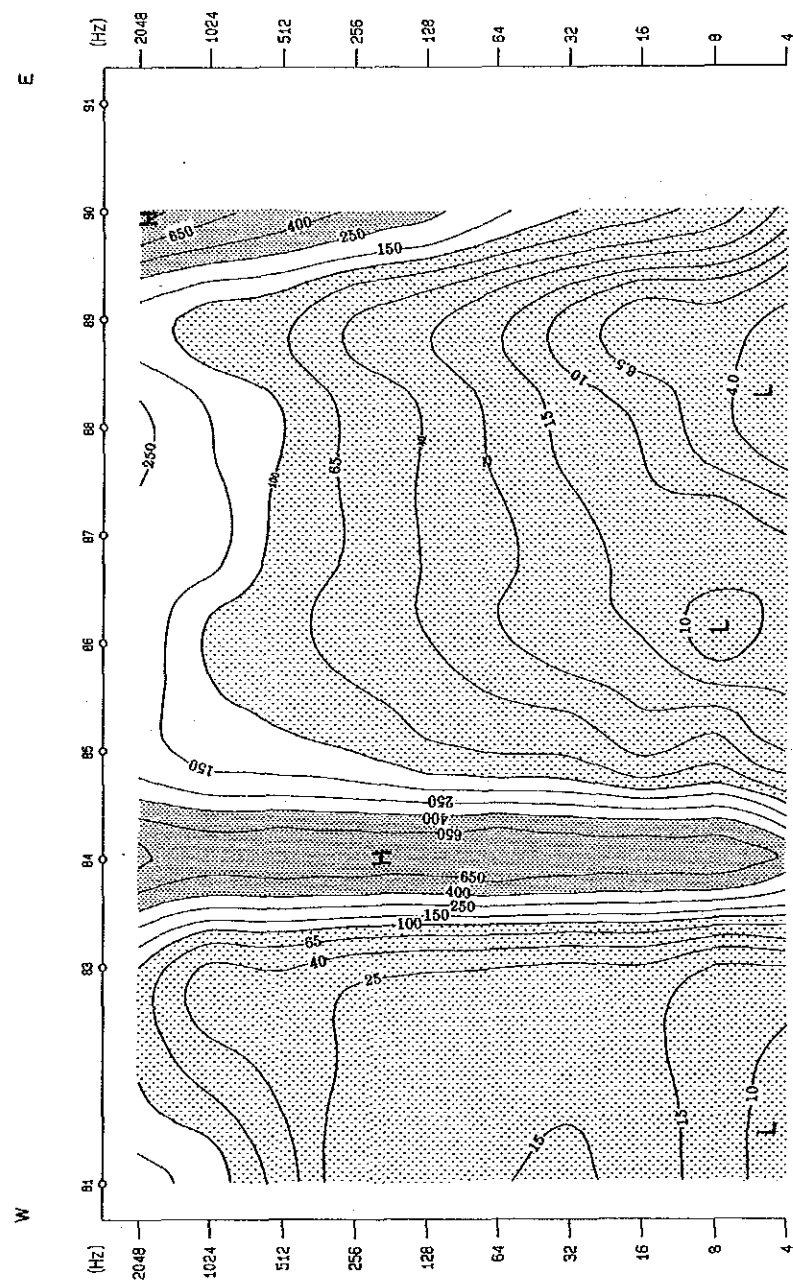


LEGEND

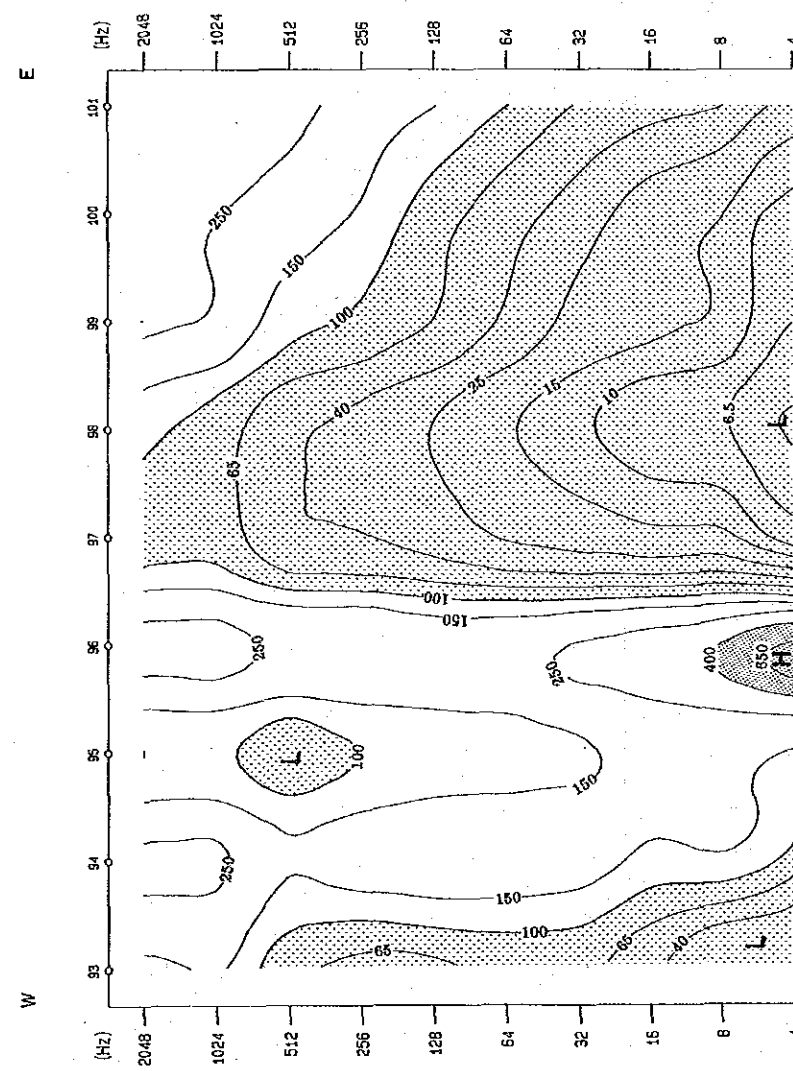
- 100 O Station and No.
- Resistivity Contour (Unit : ohm-m)
- L $\rho < 100$ ohm-m
- H 4000 ohm-m $\leq \rho$
- * ρ : Resistivity

Fig. II-2-12(3) Apparent Resistivity Section (Section-E, F)

Section - G



Section - H



LEGEND




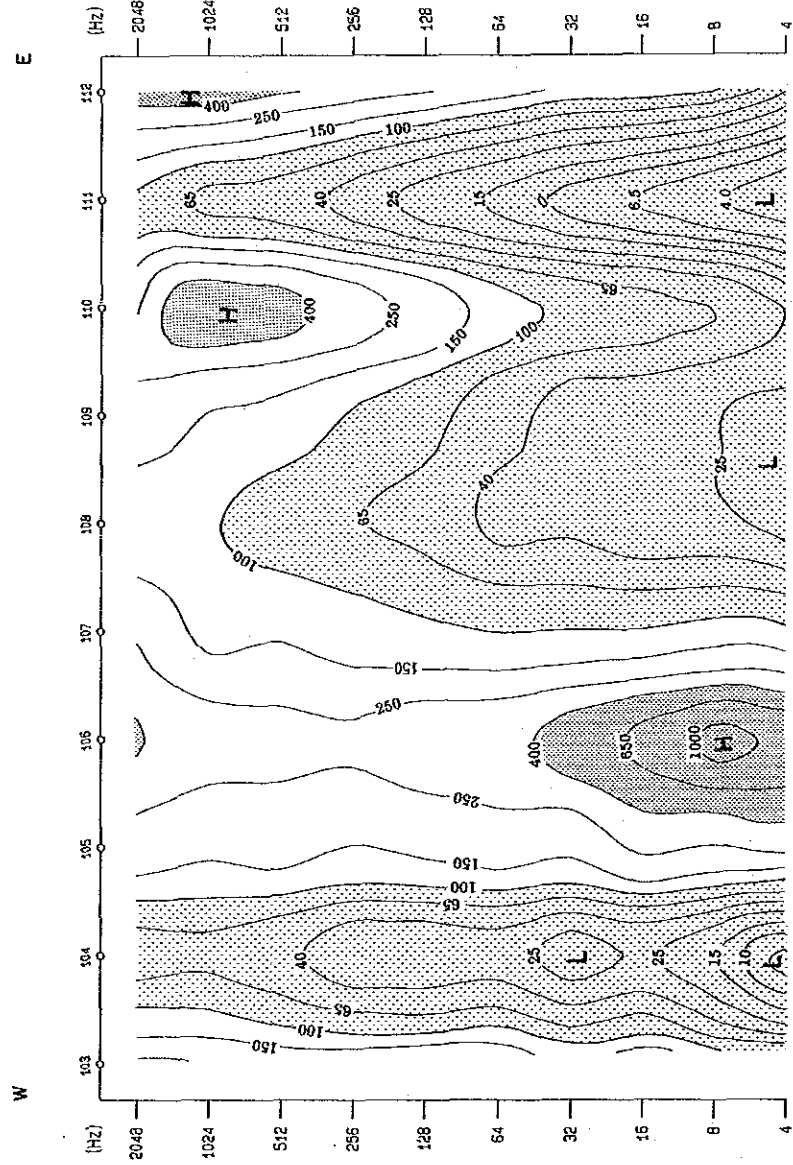
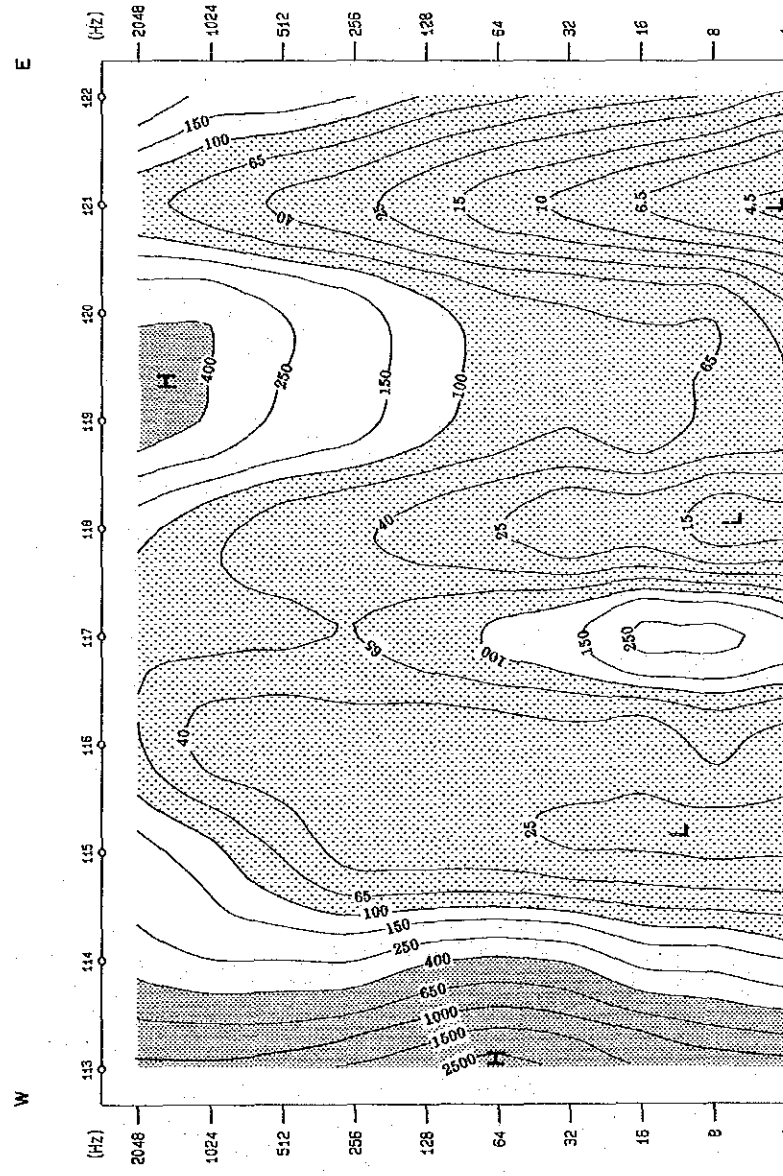
- 100 ○ Station and No.
-  Resistivity Contour
(Unit : ohm-m)
-  $\rho < 100 \text{ ohm-m}$
-  $400 \text{ ohm-m} \leq \rho$
- * ρ : Resistivity

Fig. II-2-12(4) Apparent Resistivity Section (Section-G, H)

Section - I



Section - J



LEGEND





- Station and No. 
- Resistivity Contour (Unit: ohm-m) 
- $f < 100$ ohm-m 
- 400 ohm-m $\leq f$ 
- * f : Resistivity

Fig. II-2-12 (5) Apparent Resistivity Section (Section-I, J)

- f) Western end of Line-D.
- g) Western parts of Lines-F through -G.
- h) Western end of Line-I.
- i) Eastern parts of Lines-I and -J.

Among these items, those at the item d) are observed along a creek flowing toward the south near the central part of the survey area, and show an N-S trending distribution pattern. And those at the items e), f) and g) are distributed in NNW-SSE direction each. While, those at the items h) and i) show N-S trending distribution pattern, and seem to extend toward the south beyond the survey area.

2) 512 Hz

A similar distribution pattern as that on the 1,024 Hz plan map is observed, but, several local distribution patterns are diminished in this plan map so that the distribution pattern seems to reflect a large-scale structure.

Apparent resistivities of more than 400 Ω -m are distributed at the following six parts:

- a) Central part of Line-A.
- b) Eastern end of Line-A.
- c) Western ends of Lines-B through -G.
- d) Eastern ends of Lines-D and -G.
- e) Eastern part of Line-I.
- f) Western end of Line-J.

Those at a) show a local distribution pattern smaller than that on the 1,024 Hz plan map. Those at b) and d) are distributed locally each, which are found widely on the above 1,024 Hz plan map, so that the formations causing those of more than 400 Ω -m at the both seem to be thin layers. A distribution pattern of those at c), being similar as that on the above 1,024 Hz plan map, suggests that a highly resistive rock and/or formation trending in NNW-SSE direction extends to the depth. Those at the item e) may correspond to the outer fringe of those, of which a center may be located at the west beyond the survey area. And those at the item f) show a local distribution pattern, similar as those on the above 1,024 Hz plan map.

Those of less than 100 Ω -m are distributed at the following three parts:

- g) Central part of the area.
- h) Western edges of Lines-G through -J.
- i) Eastern edges of Lines-I and -J.

Those at the item g) are a combination of those distributed at the items d) and e) on the 1,024 Hz plan map, showing a large-scale distribution pattern of "Y" shape. Since this distribution pattern shows a similar pattern as the topography at the central part, this topography seems to reflect the fault topography. While, those at the item h) show distribution patterns trending in NNW-SSE direction, being a combination of those at the items g) and h) on the 1,024 Hz plan map, and those at the item i) are distributed in N-S directions, showing a similar distribution pattern as that on the 1,024 Hz plan map. The both distribution patterns suggest to be due to the fault structures and/or accompanying fractured zones.

3) 256 Hz

A similar distribution pattern as those of the above plan maps is found.

Apparent resistivities of more than 400 $\Omega\cdot\text{m}$ are distributed at the following four parts:

- a) Central part of Line-A.
- b) Eastern edge of Line-A.
- c) Western edge of Lines-J.
- d) Eastern parts of Lines-B and -G.

Among these, those at the item d) form the largest distribution area in these above four parts, and show a similar distribution pattern trending in NNW-SSE direction as that on the 512 Hz plan map. While, those at the other three parts decrease those distribution areas than those on the 512 Hz plan map, and are found locally.

Apparent resistivities of less than 100 $\Omega\cdot\text{m}$ are concentrated at the following three parts:

- e) Central part of the survey area
- f) Southwestern part of the survey area
- g) Southeastern part of the survey area

These three low apparent resistivities show similar distribution patterns as those on the 512 Hz plan map, and the distribution areas of those are larger than those on the 512 Hz plan map. Both of those at the items e) and f) are combined at the southern part of the area, and show a distribution pattern surrounding the high apparent resistivity zone trending in NNW-SSE direction, which is distributed at the western part of the area. While, those at the item g) seem to extend to a central low-apparent-resistivity zone of large-scale at the north end.

4) 64 Hz

Low apparent resistivity zones of less than 100 $\Omega\cdot\text{m}$ are broadly distributed at the central part through the eastern part of the survey area, and seem to increase those distribution areas

towards the lower frequencies.

Apparent resistivities of more than 400 $\Omega\cdot\text{m}$ are observed at the western parts of Lines—B through —G and of Lines—I and —J. Those at the former show an NNW—SSE trending distribution pattern located between low apparent resistivity zones of less than 100 $\Omega\cdot\text{m}$. Since this distribution pattern can be observed on the above plan maps, it is suggested that highly-resistive rock and/or formation may exist at the whole depth. While, those of the latter may reflect the eastern fringe of the high resistivity layer and/or rock.

Those of less than 100 $\Omega\cdot\text{m}$ are distributed at the southwestern part and at central-to-eastern part of the survey area. Those at the former show NNE—SSW trending distribution pattern. And those at the latter occupy two-thirds of the survey area, showing a large-scale low apparent resistivity zone, in which apparent resistivities of 100 $\Omega\cdot\text{m}$ through 150 $\Omega\cdot\text{m}$ are observed locally.

5) 16 Hz

Apparent resistivities of less than 100 $\Omega\cdot\text{m}$ are broadly distributed in the survey area. And those of 100 $\Omega\cdot\text{m}$ through 150 $\Omega\cdot\text{m}$, distributed in a low apparent resistivity zones at the central-to-eastern parts of the area on the 64 Hz plan map, are diminished on this map.

Those of more than 400 $\Omega\cdot\text{m}$ are distributed at the western part and at the southwestern edge of the area, showing trends in NNW—SSE direction together. Those at the former can be found at Line—I, and seem to extend toward the southwest beyond the survey area. And those at the latter show a similar distribution pattern as those of the above plan maps, suggesting the existence of thick highly-resistive rocks.

Similar distribution pattern as that on this plan map is found on the plan maps for the frequencies of lower than 16 Hz.

(3) Physical Properties

The test of physical properties is carried out to compare observed CSAMT resistivities with resistivities of the rocks and/or formations distributed in the survey area, and to obtain the basic information for the analysis.

Resistivities of rock samples should be measured on the similar condition as those existed in the underground, so that rock samples were steeped in pure water 10 days. But as it is very difficult to put rock samples in the same condition as in the earth, some differences would be appeared between the tested and observed resistivities.

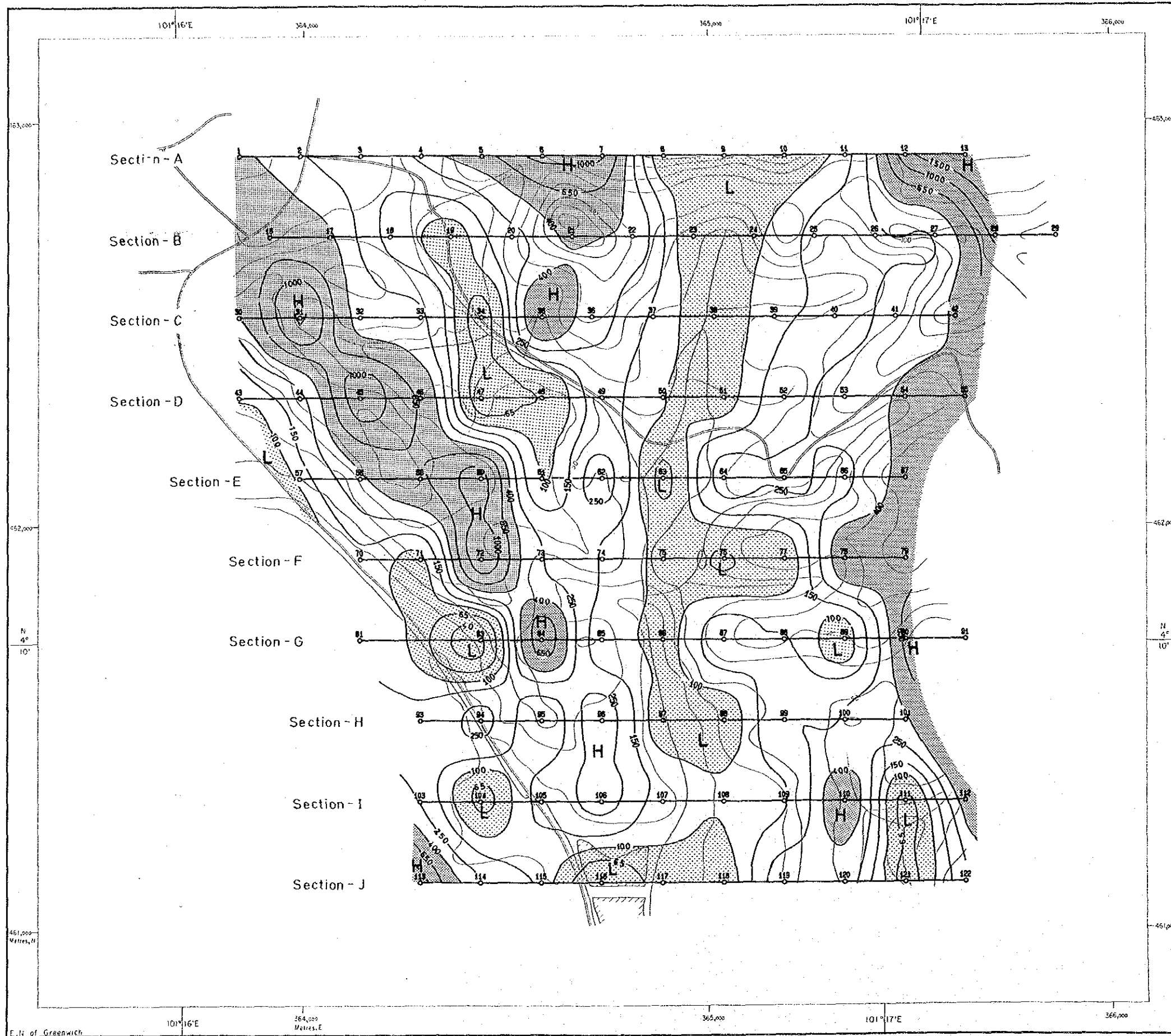
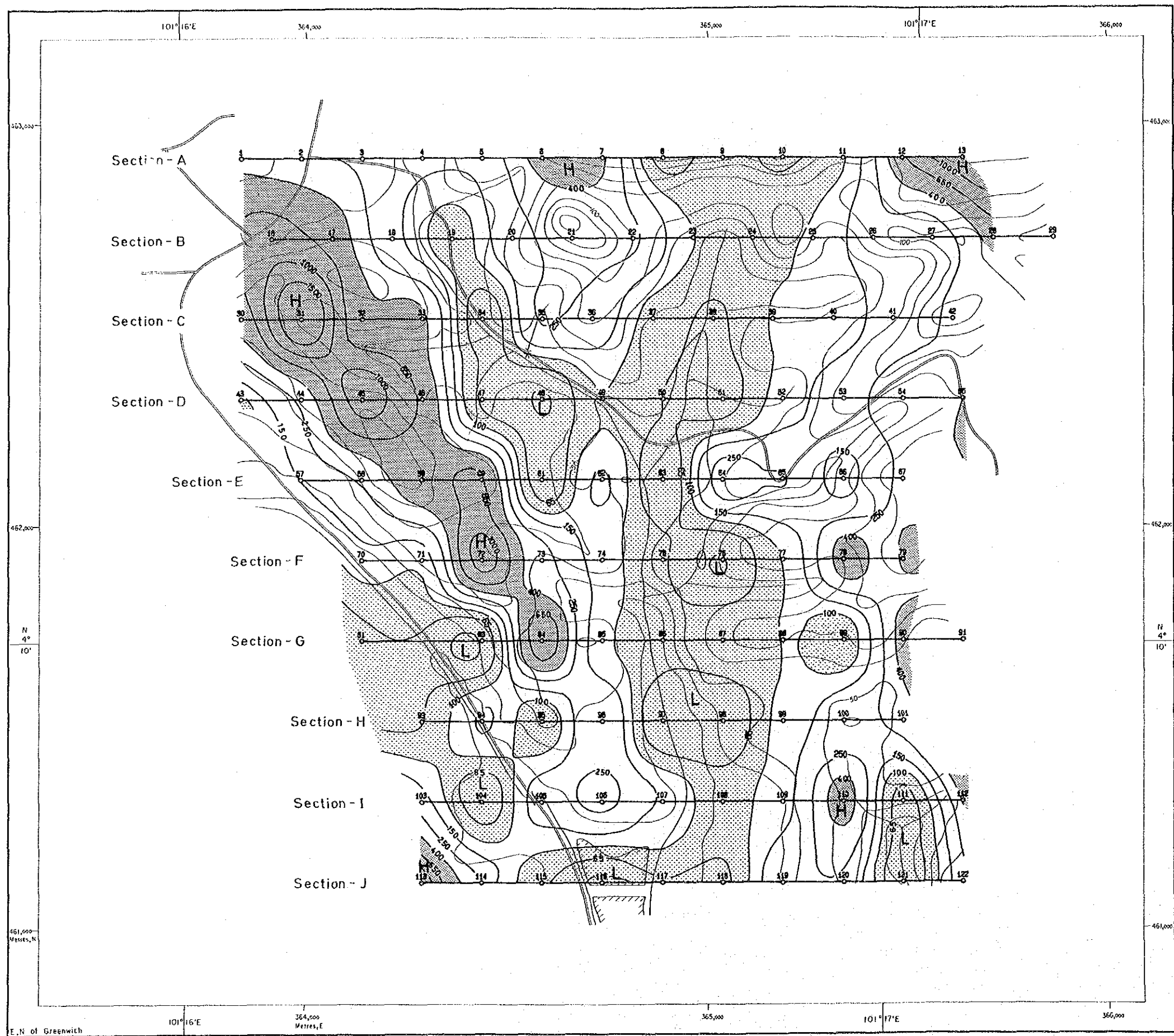
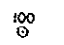






Fig. II-2-13(1) Apparent Resistivity Plan Map (1,024Hz)



LEGEND

- 
 Station and No.
- 
 Resistivity Contour
(Unit: ohm-m)
- 
 $P < 100 \text{ ohm-m}$
- 
 $400 \text{ ohm-m} \leq P$
- 
 * ρ : Resistivity

Scale 1:10,000

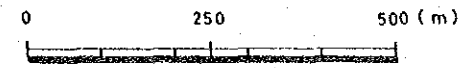
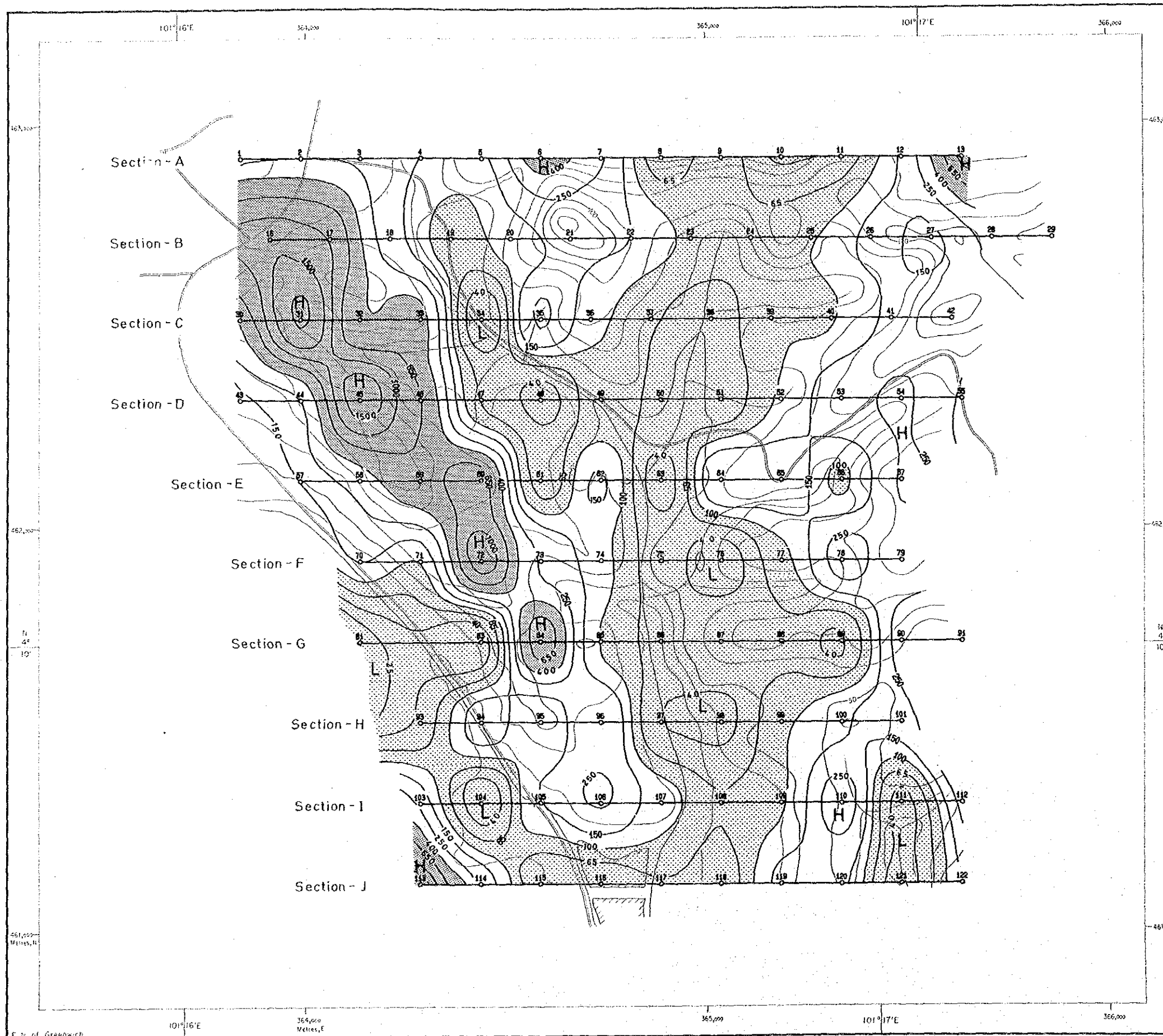
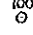





Fig. II-2-13 (2) Apparent Resistivity Plan Map (512Hz)



LEGEND

-  Station and No.
-  Resistivity Contour (Unit: ohm-m)
-  $P < 100 \text{ ohm-m}$
-  $400 \text{ ohm-m} \leq P$
- * P: Resistivity

Scale 1:10,000

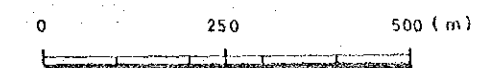
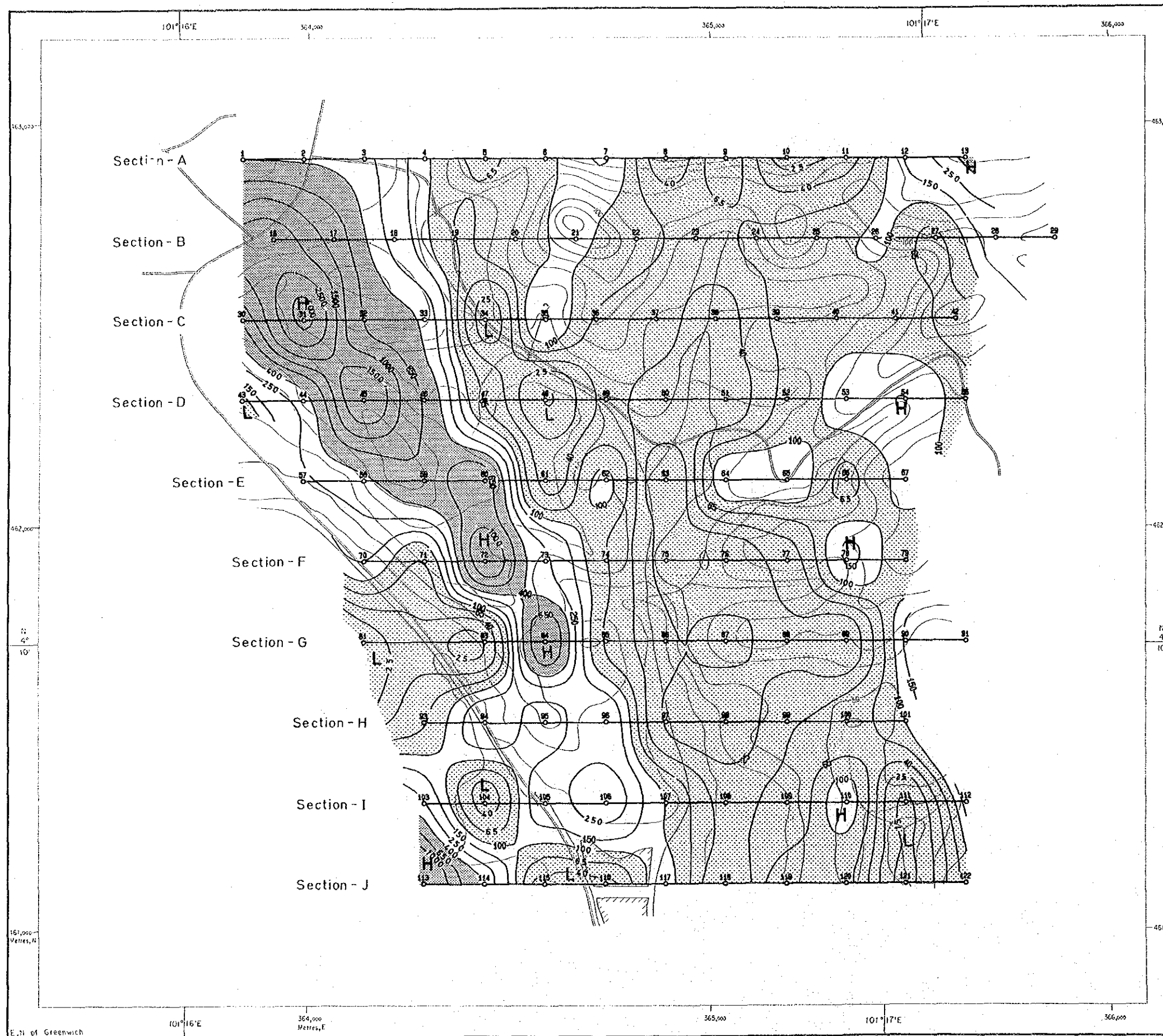


Fig. II-2-13(3) Apparent Resistivity Plan Map (256Hz)



LEGEND

- Station and No.
- Resistivity Contour (Unit: ohm-m)
- $f < 100 \text{ ohm-m}$
- $400 \text{ ohm-m} \leq f$
- ρ_f : Resistivity

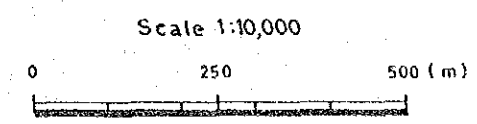
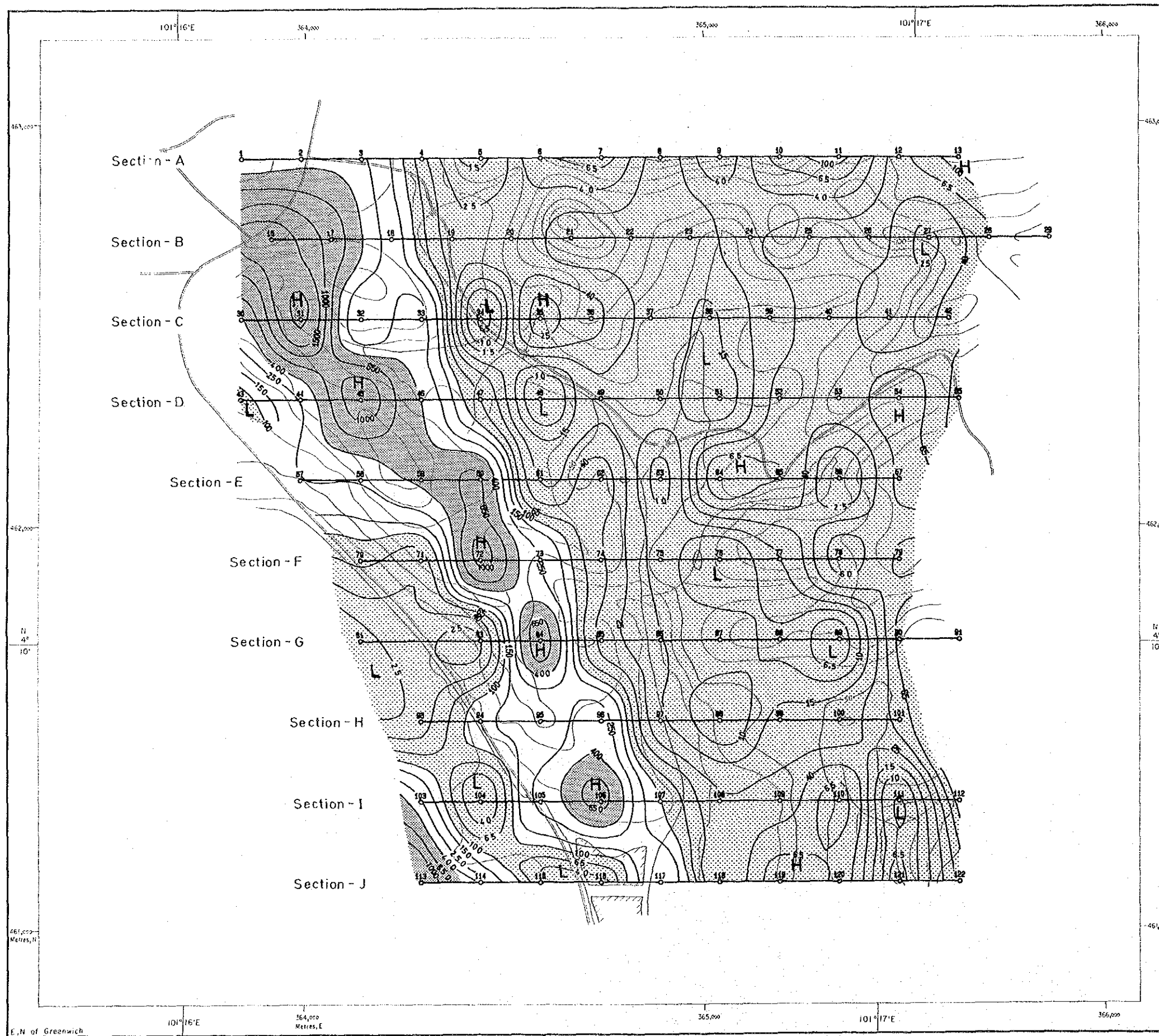
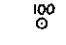





Fig. II-2-13(4) Apparent Resistivity Plan Map (64Hz)



LEGEND

- 
 Station and No.
- 
 Resistivity Contour
(Unit: ohm-m)
- 
 $\rho < 100 \text{ ohm-m}$
- 
 $400 \text{ ohm-m} \leq \rho$
- * ρ : Resistivity

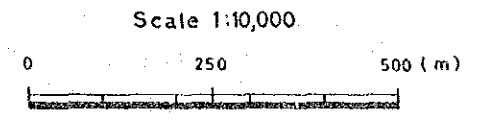


Fig. II-2-13(5) Apparent Resistivity Plan Map (16Hz)

Fifteen rock/ore samples in total were collected at the ground surface, but eleven rock/ore samples only were tested because other four samples were collapsed when steeping in pure water. Resistivity and P.F.E. of each of those samples were measured by means of Spectral IP instrument system. The results of physical property test are given in Table II-2-6.

Resistivities of eleven rock samples are 529 $\Omega\cdot m$ to 7,260 $\Omega\cdot m$, and average value of those is 3,223 $\Omega\cdot m$.

Average value of each rock/ore is shown below.

Rock Name	Resistivity in $\Omega\cdot m$	P.F.E. in %	Number of samples
Iron oxide ore	2,843	4.6	4
Meta sandstone	1,342	1.9	4
Quartz vein	7,441	0.8	2
Quartz schist	1,137	1.9	1

- 1) Iron oxide ore shows resistivity between 578 $\Omega\cdot m$ and 7,260 $\Omega\cdot m$, and higher P.F.E. than other rocks.
- 2) Metasandstone shows similar resistivity value as that of quartz schist.
- 3) Quartz vein shows the highest resistivity among all rocks.

Therefore, the high resistivity zone observed in this survey may correspond to the distribution area of metasandstone, quartz vein and quartz schist.

Table II-2-6 Electrical Properties of Rock Samples

Sample Number	Resistivity in $\Omega\cdot m$	Phase Difference in -mrad	P.F.E. in %	Rock Name
B-17	2,474	51	7.1	Iron oxide ore
B-23.5	1,170	9	1.2	Meta sandstone
B-23.6	1,137	13	1.9	Quartz schist
E-57.5	1,060	5	0.9	Iron oxide ore
E-63	2,344	15	2.2	Meta sandstone
F-72	578	50	6.0	Iron oxide ore
F-74.5	1,742	14	2.1	Meta sandstone
H-96	5,630	7	0.9	Quartz vein
H-99.75	7,260	37	4.5	Iron oxide ore
I-117.5	9,252	4	0.6	Quartz vein
I-111.5	1,720	17	2.7	Metasandstone

(4) Resistivity Sections

Using the results of 1-D analysis in which a horizontal multi-layer earth model is presumed, 2-D resistivity structure up to -1,000 m S.L. below each of ten survey lines is illustrated. The ten resistivity sections are shown in Figures II-2-14(1) to II-2-14(5).

1) Section-A

This section shows different structures at the both sides of station 5. A single-layer structure of high resistivity is distributed at the west of station 5, and a two-layer structure of shallow-high and deeper-low is found at the east.

A high resistivity layer of 200 $\Omega\cdot\text{m}$ through 500 $\Omega\cdot\text{m}$ are distributed up to the depth of shallower than -1,000 m G.L. at the west of station 5.

Between stations 5 and 7, a three-layer structure is observed, in which the resistivities of the first, second and third layers are 3,000 $\Omega\cdot\text{m}$, 100 $\Omega\cdot\text{m}$ and 50 $\Omega\cdot\text{m}$, respectively.

Between stations 7 and 11, a two-layer structure is found, in which the resistivity and thickness of the first layer are of more than 100 $\Omega\cdot\text{m}$ and about 120 m, respectively, and the resistivity of the second layer is of less than 50 $\Omega\cdot\text{m}$.

And at the east of station 11, a two-layer structure is observed, in which the resistivity and thickness of the first layer are of more than 1,500 $\Omega\cdot\text{m}$ and about 250 m respectively, and the resistivity of the second layer is of less than 50 $\Omega\cdot\text{m}$.

The four resistivity discontinuities are observed around station 5, around station 7, between stations 8 and 9, and around station 11. Among these discontinuities, the one around station 5 shows a strongest resistivity contrast.

2) Section-B

This section shows a similar structure as that in the Section-A, and it is suggested that the resistivity structure shown in the Section-A extends toward the south. While, the upper layers at the central to eastern parts are thicker than those in the Section-A.

At the west of station 17, a two-layer structure is found, in which the resistivity and thickness of the first layer are of 500 $\Omega\cdot\text{m}$ through 700 $\Omega\cdot\text{m}$ and 200 m respectively, and the second layer shows the resistivity of more than 2,000 $\Omega\cdot\text{m}$. Similar resistivity values as that of the first layer can be observed in the first layers between stations 20 and 22, and between 24 and 27, and in the second layer at the east of station 27.

At the east of station 17, two- or three-layer structures are found. The resistivities of the first layers between stations 17 and 19, between 19 and 23, between 23 and 24, between 24 and

27, and at the east of station 27 are of 100 $\Omega\cdot\text{m}$ through 250 $\Omega\cdot\text{m}$, 500 $\Omega\cdot\text{m}$ through 1,000 $\Omega\cdot\text{m}$, 100 $\Omega\cdot\text{m}$, 250 $\Omega\cdot\text{m}$ through 500 $\Omega\cdot\text{m}$ and 2,000 $\Omega\cdot\text{m}$, respectively. And the second and/or third layers are the low resistivity layers of less than 20 $\Omega\cdot\text{m}$, except for 250 $\Omega\cdot\text{m}$ of the second layer between stations 19 and 23, and 500 $\Omega\cdot\text{m}$ of the second layer at the east of station 27.

3) Section—C

The resistivity structure on this section shows a similar structure as the ones observed in the Sections A and B except for local high-resistivity layers at the shallower part, so that the continuity of the resistivity structure in N—S direction is suggested.

At the west of station 34, a thick layer of high resistivity of more than 300 $\Omega\cdot\text{m}$ is observed. In particular, at the west of station 32, this layer shows a thickness of more than 1,000 m. Moreover, high resistivity layers of more than 1,000 $\Omega\cdot\text{m}$ are observed in the second layer at the west of station 31, and in the first layers of between stations 30 and 32, and of between 34 and 36.

Between stations 34 and 40, a three-layer structure is found, in which the resistivities of the first and second layers are of 100 $\Omega\cdot\text{m}$ through 200 $\Omega\cdot\text{m}$ and the lowest layer shows a resistivity of 20 $\Omega\cdot\text{m}$ through 50 $\Omega\cdot\text{m}$. And at the east of station 40, a two-layer structure is distributed, in which the first layer shows the resistivity of 300 $\Omega\cdot\text{m}$ through 500 $\Omega\cdot\text{m}$ and the thickness of between 200 m and 250 m, and the second layer is a low resistivity layer of 20 $\Omega\cdot\text{m}$ through 50 $\Omega\cdot\text{m}$.

4) Section—D

On this section, the first highly-resistive layers distributed locally at the central parts of Sections—A through —C, are diminished, and a resistivity layer of 100 $\Omega\cdot\text{m}$ through 500 $\Omega\cdot\text{m}$ becomes thinner than that found at the central-eastern part of each of three sections, A, B and C.

At the west of station 46, a resistivity layer of 100 $\Omega\cdot\text{m}$ through 850 $\Omega\cdot\text{m}$ with a thickness of more than 1,000 m is observed. And a resistivity layer of 70 $\Omega\cdot\text{m}$, seemed to be due to the fractured zones developed at the boundary between granite and phillite, is found at the western edge of the above layer.

Between stations 46 and 52, a two-layer structure is observed, in which the resistivities of the first and second layers are of 100 $\Omega\cdot\text{m}$ through 500 $\Omega\cdot\text{m}$ and of 15 $\Omega\cdot\text{m}$ through 40 $\Omega\cdot\text{m}$, respectively.

At the east of station 52, a three-layer structure is observed in which the first layer shows a resistivity of 1,000 $\Omega\cdot\text{m}$ and the second layer is the same one as the first layer of between stations 46 and 52.

5) Section--E

This section shows the different resistivity structures at the both sides of station 61 at the central part.

At the western side, a three-layer structure is found. In this structure, a high resistivity layer of more than 200 $\Omega\cdot\text{m}$, seemed to reflect a thick highly-resistive rock and/or formation, is distributed at the whole depth. As the resistivity in this layer vary greatly and show higher value in the depth, this layer seems to be unhomogeneous. And a lot of resistivity discontinuities are presumed in the western side.

On the other hand, at the eastern side of station 60, a two-layer structure is observed, in which the resistivities of the first and second layers are of 100 $\Omega\cdot\text{m}$ through 400 $\Omega\cdot\text{m}$ and of less than 50 $\Omega\cdot\text{m}$, respectively. The thickness of the first layer increases towards the east gradually, that is, about 100 m around stations 61, about 150 m between stations 61 and 63, and about 200 m at the east of station 64. This eastward increase suggests that the fault structures inferred at station 61, and between stations 63 and 64 dip towards the west.

6) Section--F

This section shows a two-layer structure except for the western part, where a vertical high-resistivity layer seemed to reflect dyke is found.

A high-resistivity layer found at the western part (between stations 71 and 73) seems to be an extension of that at the western part of each of the above sections, but decreases its width sharply in this section. Judging from the amount of resistivity discontinuities within this high resistivity layer, this decrease in width may be caused by the decrease in resistivity reflecting the fracture zones accompanied by the fault structures.

Between stations 72 and 78, a two-layer structure is observed, in which the first layer shows the resistivity of 100 $\Omega\cdot\text{m}$ through 300 $\Omega\cdot\text{m}$ and the thickness of 250 m through 400 m, and the second layer is a low resistivity layer of 15 $\Omega\cdot\text{m}$ through 20 $\Omega\cdot\text{m}$. At the east of station 78, a three-layer structure is found: the first layer shows the resistivity of 500 $\Omega\cdot\text{m}$ and the second layer is the same one as the above first layer. The resistivity structure between stations 72 and 78 seems to reflect local variations in resistivity only.

A resistivity layer of less than 40 $\Omega\cdot\text{m}$ is widely distributed at the deepest part, but this layer is divided by a vertical highly-resistive layer found around station 72. This layer distributed at the west of station 72, which is found locally in the depth in the above-mentioned sections, shows the width of more than 200 m and seems to extend toward the west. The increase in resistivity of this western low-resistivity layer/rock seems to be due to the existence of a large

amount of fracture zones and/or argillization accompanied by the fault structures.

7) Section—G

This section shows a two-layer structure except for station 84, and the thickness of the first high-resistivity layers are thinner than those in the Section—F.

The first layers are divided by several resistivity discontinuities, and those thickness are of 100 m more or less. And the second layers show low resistivity of 20 $\Omega\cdot\text{m}$ through 30 $\Omega\cdot\text{m}$.

At station 84, a vertical high-resistivity layer/rock is found, which corresponds to a southern extension from the Section—F.

8) Section—H

The whole resistivity structure shows a similar one as that in the Section—G, except that a vertical high-resistivity layer/rock increases its width in this section.

At the west of station 94, a two-layer structure is observed, in which the first layer shows resistivity of 200 $\Omega\cdot\text{m}$ through 300 $\Omega\cdot\text{m}$ and thickness of 80 m, and the second layer is a low resistivity layer of 20 $\Omega\cdot\text{m}$ through 50 $\Omega\cdot\text{m}$. While, at the east of station 97, a similar two-layer structure as that at the west of station 94, is distributed, which is composed of the first layer with resistivity of 200 $\Omega\cdot\text{m}$ through 300 $\Omega\cdot\text{m}$ and thickness of 100 m through 200 m, and the second layer of resistivity of 20 $\Omega\cdot\text{m}$ through 30 $\Omega\cdot\text{m}$.

Between stations 95 and 96, a three-layer structure is shown, in which the resistivity and thickness of the first layer are of 100 $\Omega\cdot\text{m}$ through 300 $\Omega\cdot\text{m}$ and of about 170 m, respectively, and the middle and lowest layers show resistivity of more than 800 $\Omega\cdot\text{m}$. Since the resistivity in this part shows higher value in the depth, it seems that the formation and/or rock in the depth is compact and homogeneous.

At the east of station 100, a two-layer structure is observed, which is composed of the first layer with the thickness of 200 m and resistivity of 500 $\Omega\cdot\text{m}$, and the second low-resistivity layer of 20 $\Omega\cdot\text{m}$ through 30 $\Omega\cdot\text{m}$.

9) Section—I

In this section, many resistivity discontinuities are found, and the resistivity structures are notably clustered into blocks.

At the west of station 104, a low resistivity layer of 15 $\Omega\cdot\text{m}$ through 50 $\Omega\cdot\text{m}$ is predominantly distributed, except that a resistivity layer of 200 $\Omega\cdot\text{m}$ is found at the shallower part of station 103.

Between stations 104 and 106, a two-layer structure is observed, which is composed of the first layer with thickness of more than 400 m and resistivity of 100 $\Omega\cdot\text{m}$ through 300 $\Omega\cdot\text{m}$, and the second layer with high resistivity of 1,000 $\Omega\cdot\text{m}$. These high resistivity layer/rock are the southern extension of vertical high-resistivity rocks observed in the Section--H, and those width are larger than those in the Section--H.

At the east of station 106, a two-layer structure is observed, in which resistivities of the first and second layers are of 100 $\Omega\cdot\text{m}$ through 500 $\Omega\cdot\text{m}$ and of 15 $\Omega\cdot\text{m}$ through 50 $\Omega\cdot\text{m}$. The thickness of the first layer increases toward the east, but it varies greatly due to the existence of several resistivity discontinuities (fault structures).

Low resistivity layer/rock of 15 $\Omega\cdot\text{m}$ through 50 $\Omega\cdot\text{m}$ observed at the west of station 104 seems to be due to the existence of fault structures, which may correspond to the boundary between granite and compact sandstone including quartz. Therefore, it is suggested that a resistivity layer of 200 $\Omega\cdot\text{m}$, distributed in the shallower part at the west of station 103, and high resistivity layers of more than 100 $\Omega\cdot\text{m}$, distributed between stations 104 and 106, are not caused by the same geology.

10) Section--J

At the western edge of the section, a high resistivity layer/rock of more than 1,000 $\Omega\cdot\text{m}$, thought to correspond to granite, is distributed at the whole depth. While, at the east of station 108, a two-layer structure is observed, in which the resistivities of the first and second layers are of 300 $\Omega\cdot\text{m}$ and of 10 $\Omega\cdot\text{m}$ through 50 $\Omega\cdot\text{m}$ respectively.

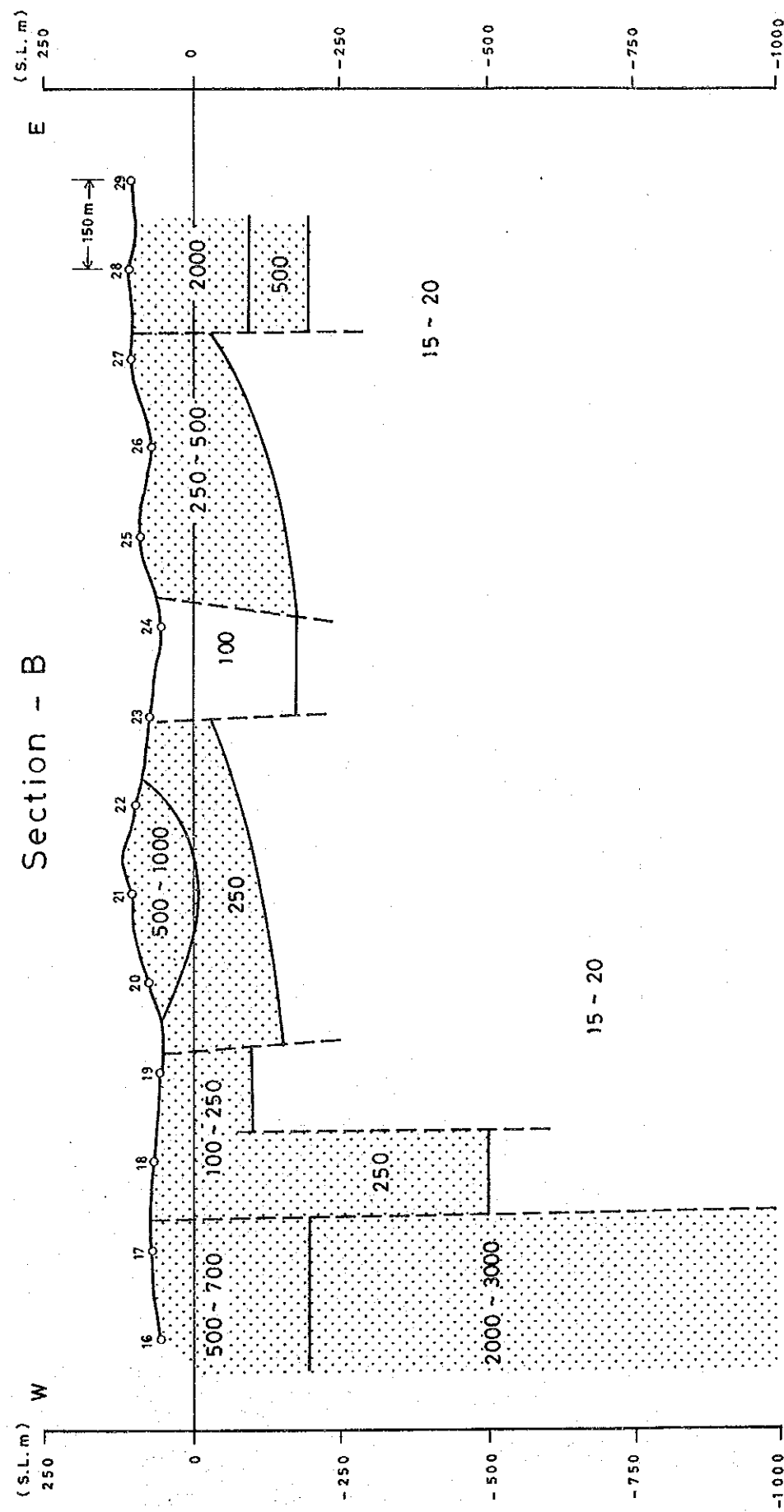
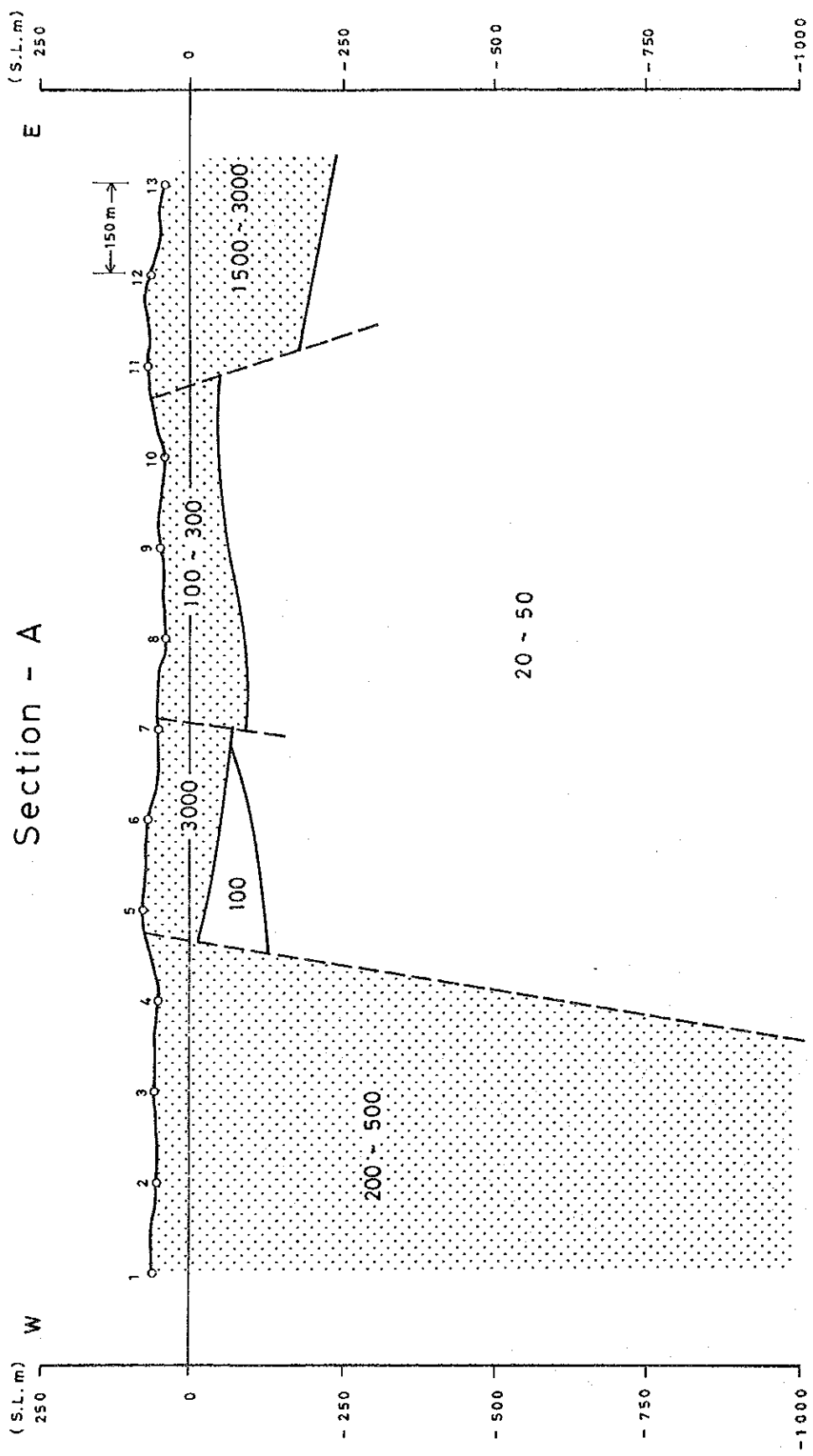
A low resistivity layer of 20 $\Omega\cdot\text{m}$, seemed to correspond to geological boundary, is distributed at the depth around station 115.

Between stations 116 and 117, a resistivity layer of 50 $\Omega\cdot\text{m}$ through 70 $\Omega\cdot\text{m}$ is observed at the shallower part, which reflects swamps and/or ponds distributed at the ground surface. And a deeper layer of resistivity of more than 700 $\Omega\cdot\text{m}$ is a southern extension of a high resistivity layer found between stations 105 and 106 in the Section--I.

(5) Resistivity Plan Maps

The resistivity plan map represents the plane distribution of the resistivity structure at some level, and in this survey, the plan map was made at each level of -50 m G.L., -100 m G.L. and -200 m G.L., taking the existed geological and geochemical information in this area into consideration. Each of the three plan maps is shown in Figure II-2-15(1) through II-2-15(3).

Resistivity distribution in the shallower part in the survey area is clearly divided into three



LEGEND

- Station and No.
- High Resistivity Layer
- Lateral Resistivity Discontinuity Line
- 1000 Resistivity Value of the Layer Aridized

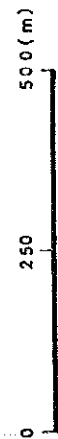
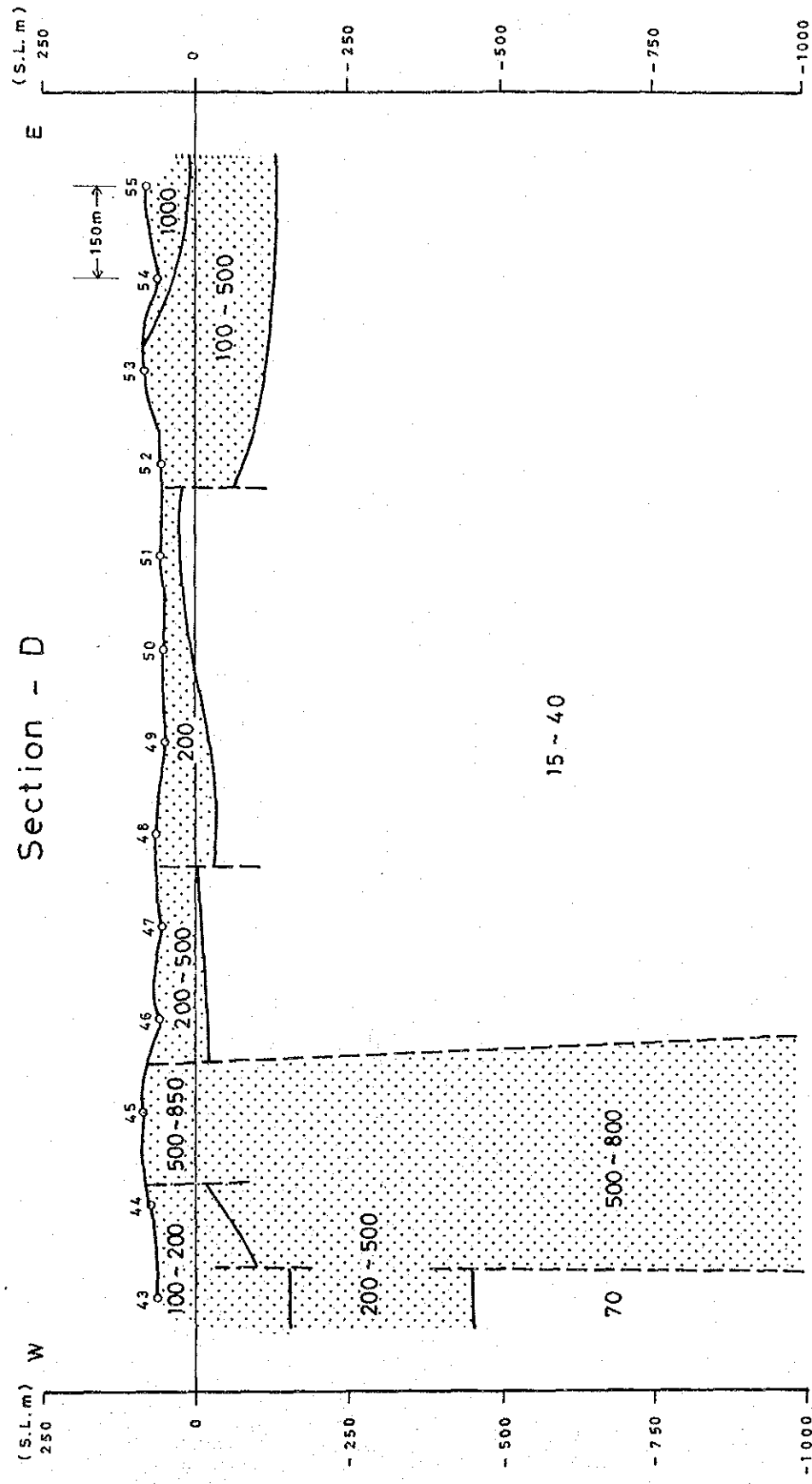
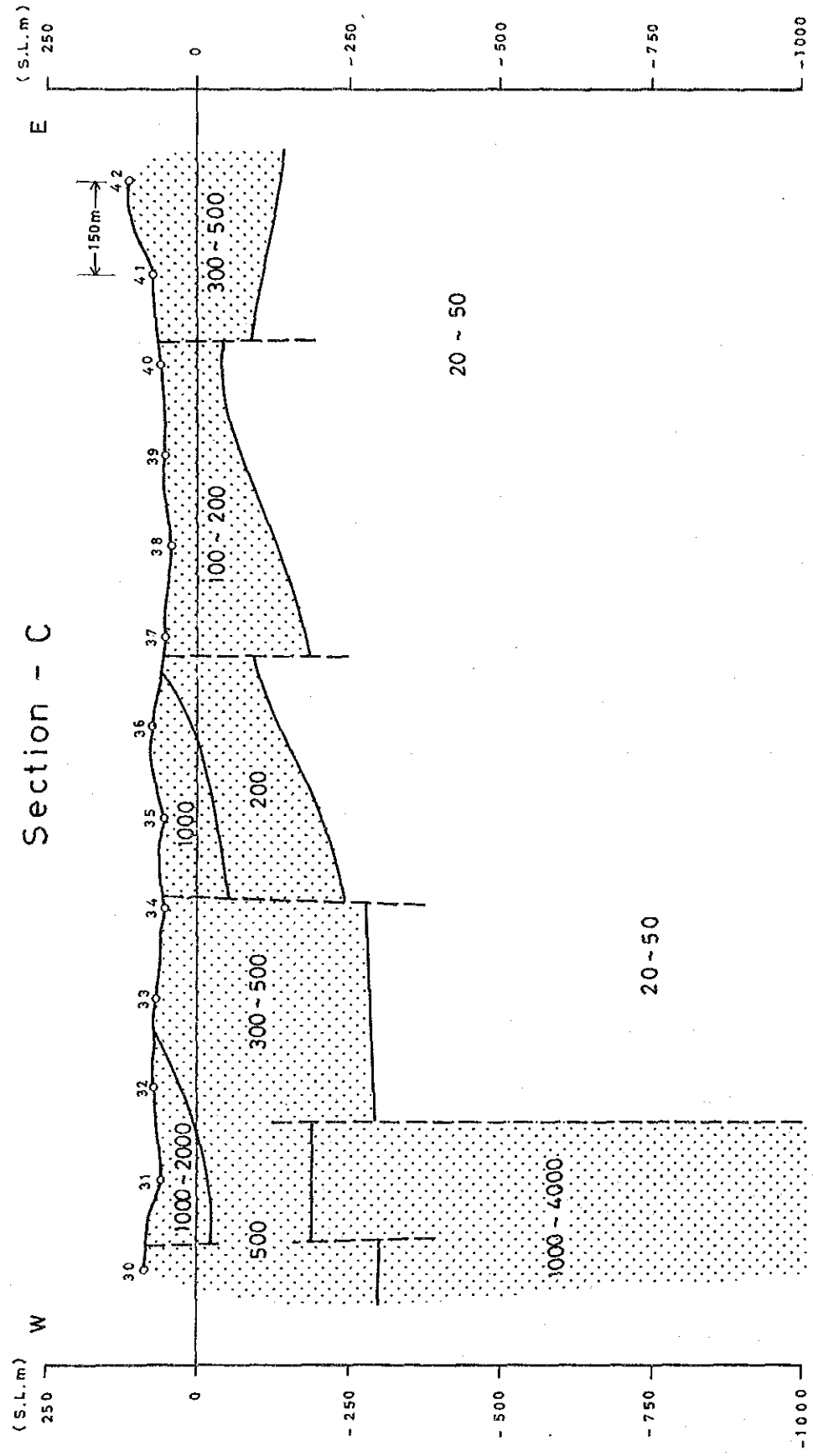


Fig. II-2-14(1) Resistivity Section (Section-A, B)



LEGEND

- Station and No.
- High Resistivity Layer
- Lateral Resistivity Discontinuity Line
- Resistivity Value of the Layer Analyzed

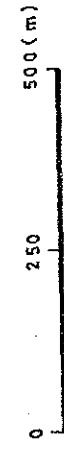
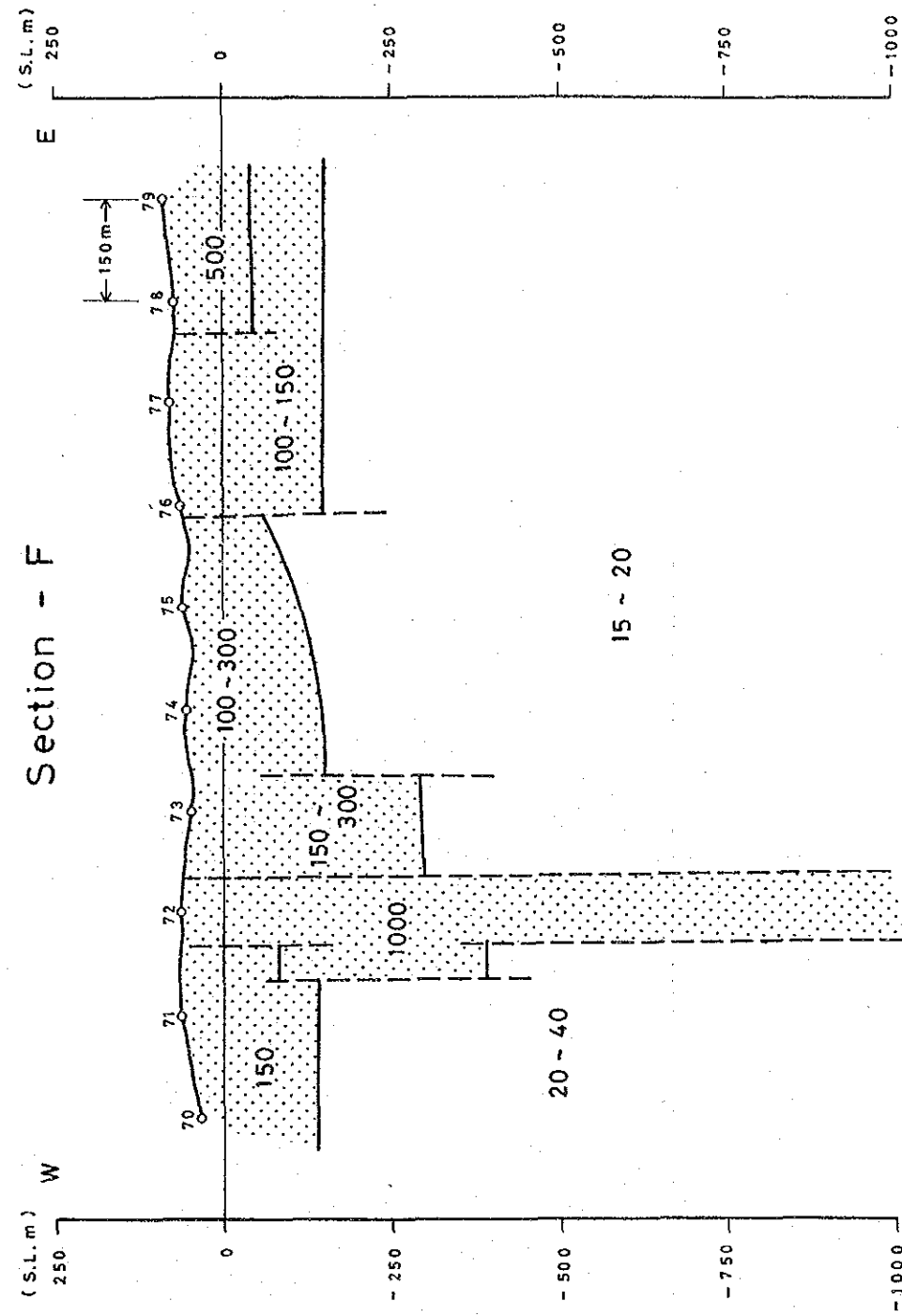
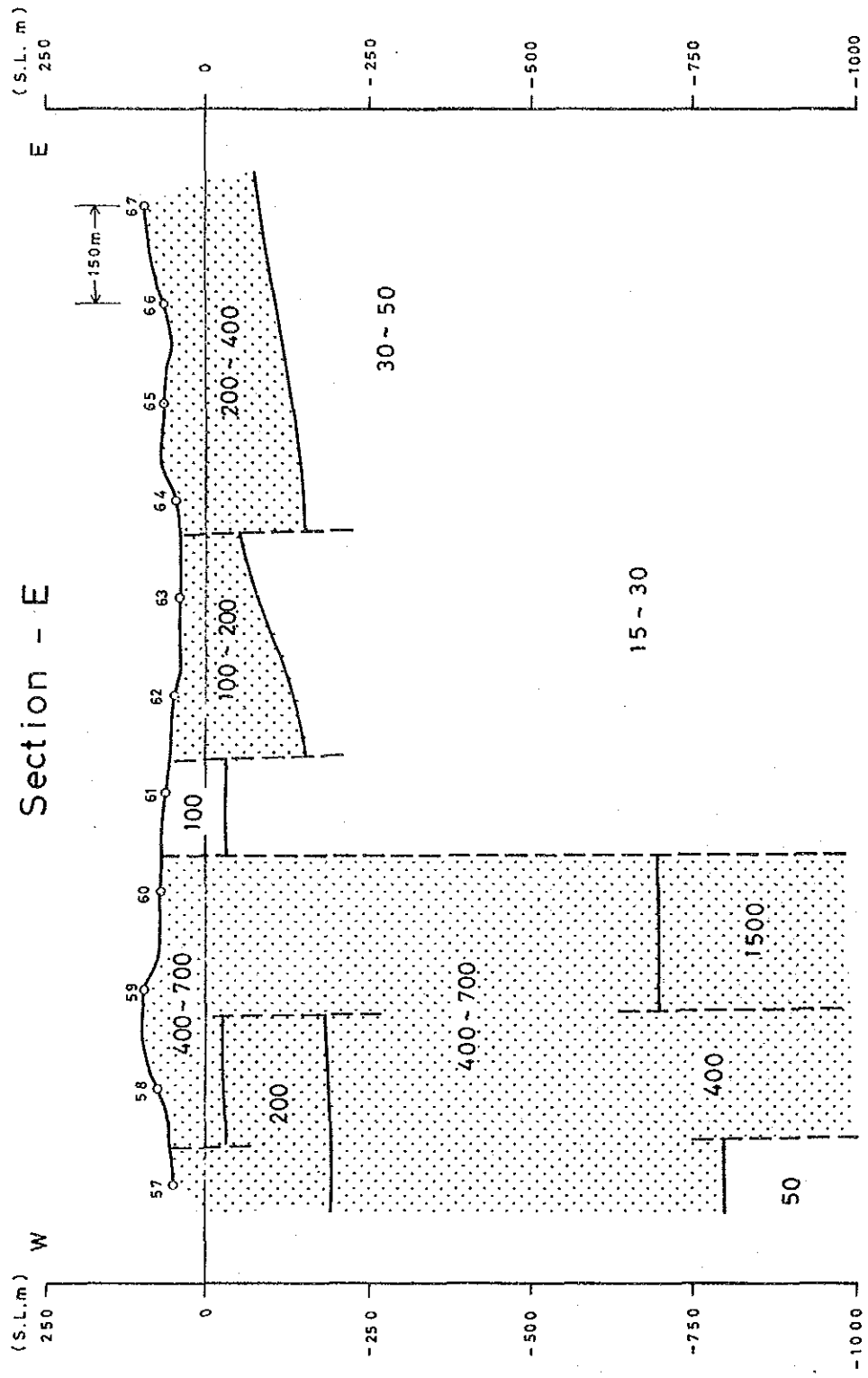


Fig. II-2-14(2) Resistivity Section (Section-C, D)



LEGEND

- Station and No.
- High Resistivity Layer
- Lateral Resistivity Discontinuity Line
- Resistivity Value of the Layer Analyzed

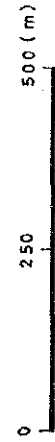
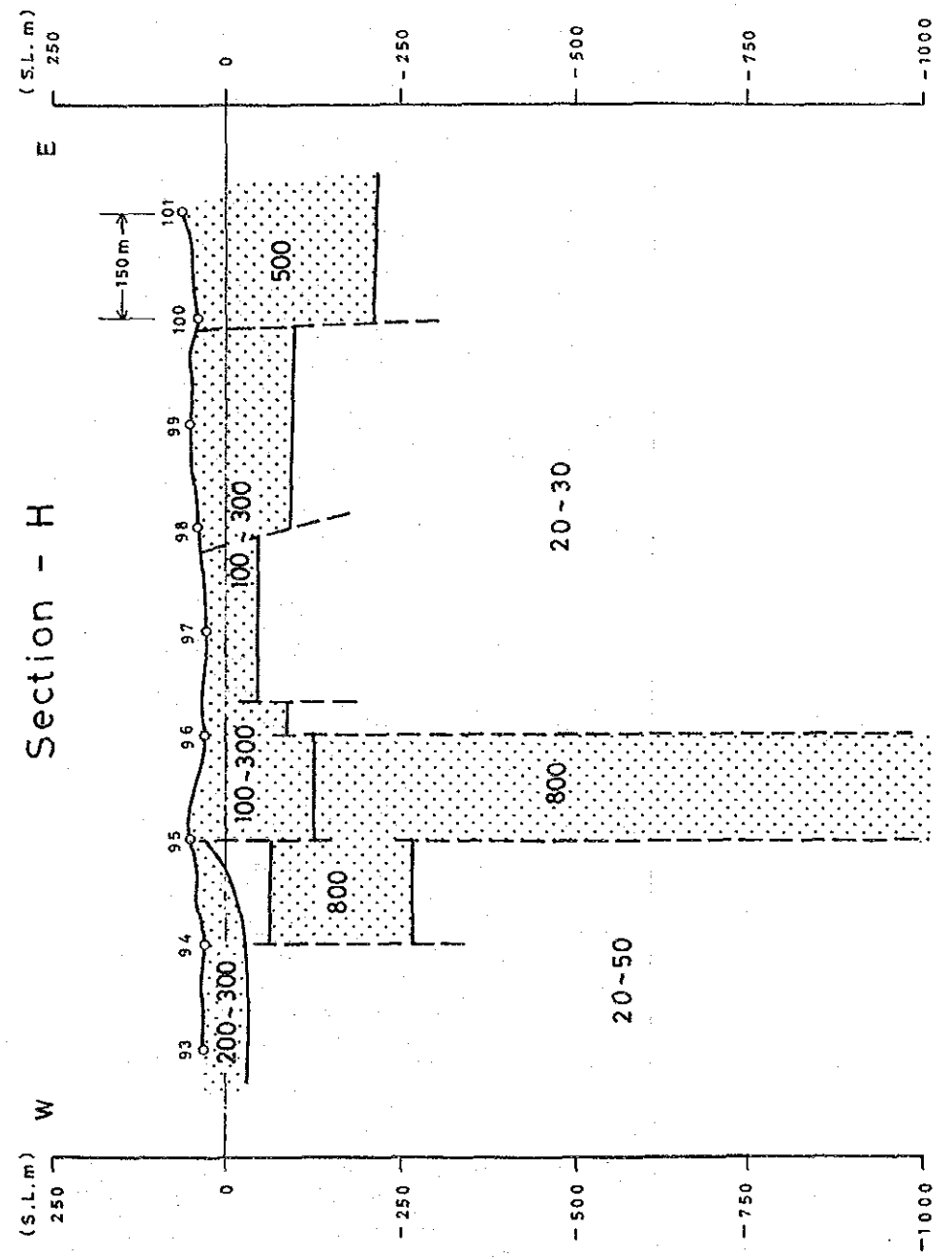
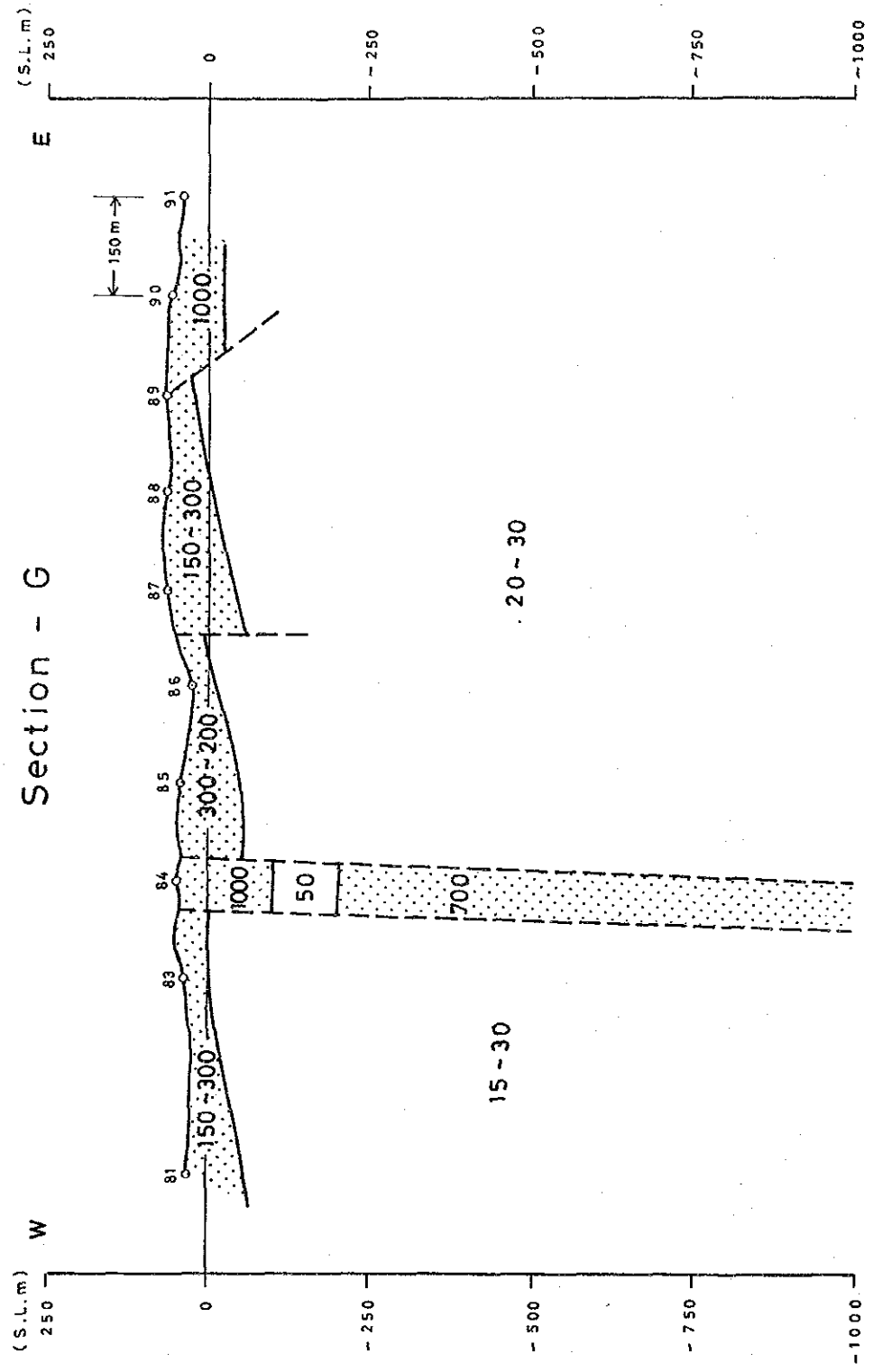


Fig. II-2-14 (3) Resistivity Section (Section-E, F)

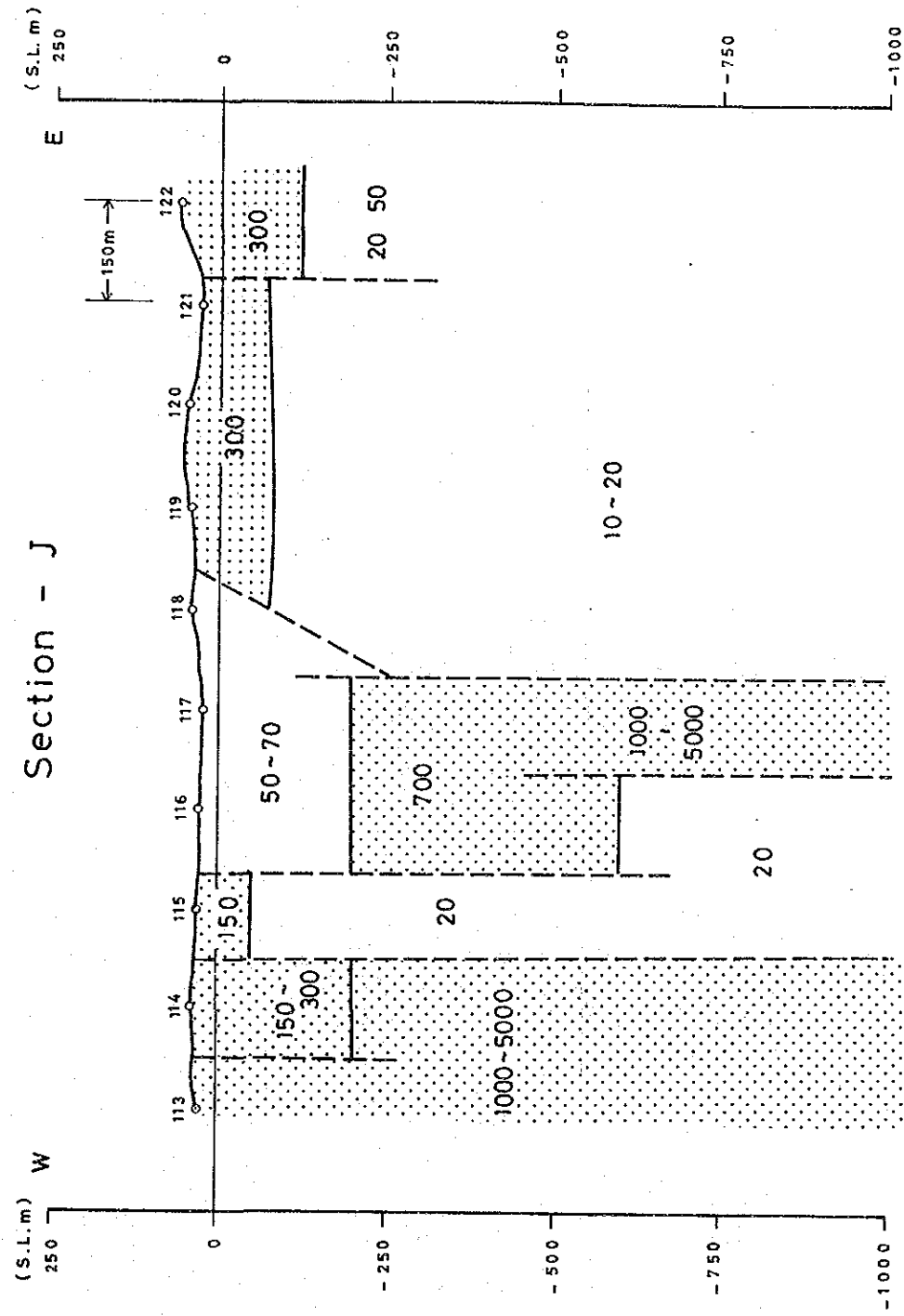
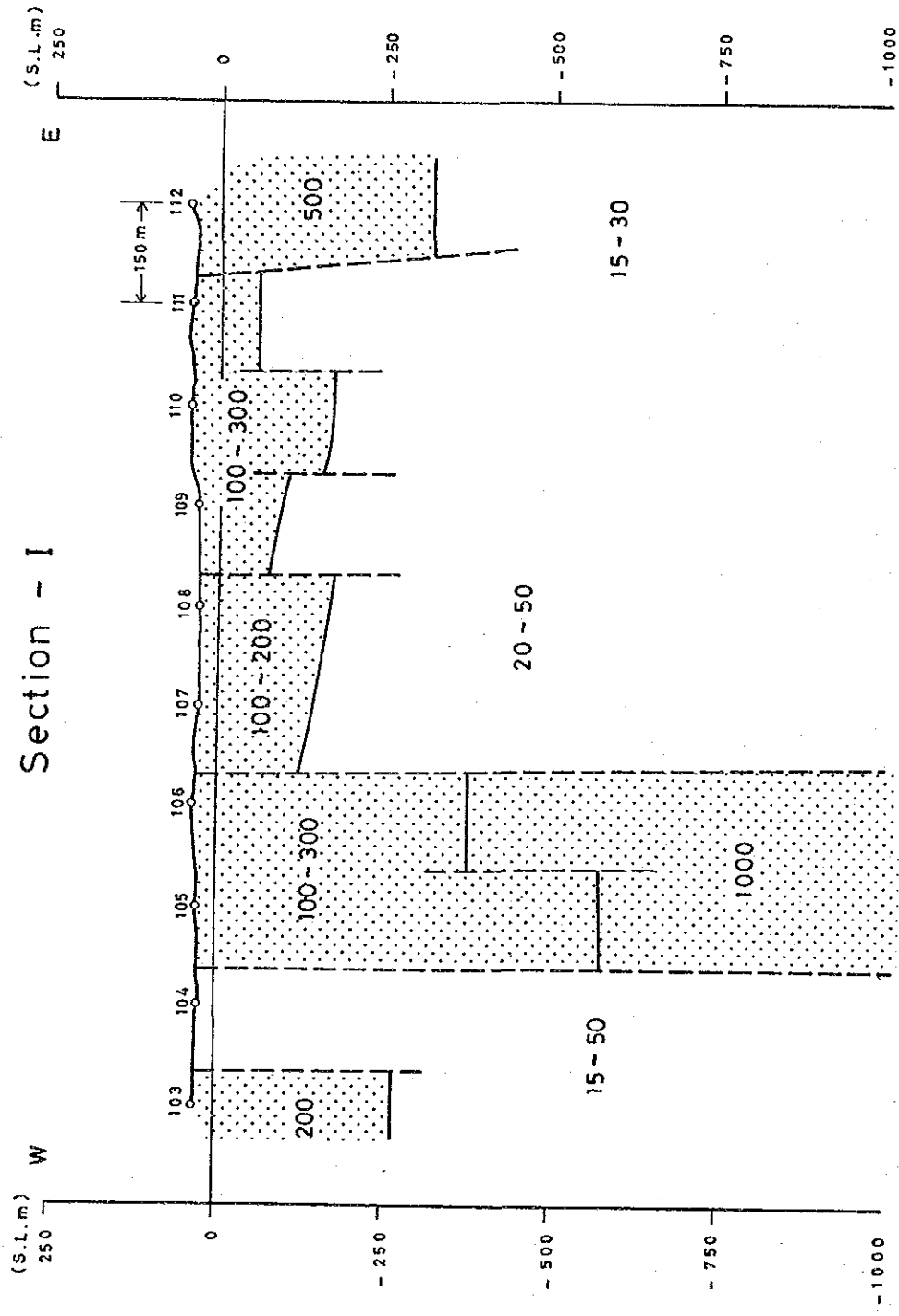


LEGEND

- Station and No.
- High Resistivity Layer
- Lateral Resistivity Discontinuity Line
- 1000 Resistivity Value of the Layer Analyzed



Fig. II-2-14(4) Resistivity Section (Section-G, H)



LEGEND

- Station and No.
- High Resistivity Layer
- Lateral Resistivity Discontinuity Line
- Resistivity Value of the Layer Analyzed



Fig. II-2-14 (5) Resistivity Section (Section-I, J)

zones, namely, high-low-high resistivity zones from the west toward the east. But the low resistivity zone increases its distribution area toward the depth so that resistivity is lowered to the depth.

In making a discussion of the plane resistivity distributions at three levels, resistivities are classified into the following three ranges:

High resistivity	more than 400 $\Omega\cdot m$
Medium resistivity	100 $\Omega\cdot m$ through 400 $\Omega\cdot m$
Low resistivity	less than 100 $\Omega\cdot m$

1) -50 m G.L. (Figure II-2-15(1))

High and low resistivity zones are cut by notable discontinuity lines, showing no continuities between those zones. In particular, low resistivity zones reflect this tendency.

High resistivity zones are observed at the western, central-northern and eastern parts of the survey area. Among those, the western zone is distributed in NNW-SSE direction, and extends to the central part at the southern end of the zone. The central-northern zone, of which the southern limits is observed around the Line-C, shows an extension toward the north beyond the survey area, and also extends to the western zone at the northern edge of the zone. While, the eastern zone is distributed at the eastern edge of each of the Lines-A through -J, and shows a tendency to extend toward the east beyond the survey area.

Low resistivity zones are distributed at the central and southern parts of the area. The central zone is composed of six independent zones in small scale, and the arrangement of these small zones suggests the existence of geotectonic lines. Among these geotectonic lines, the notable ones run in NNW-SSE direction from the northwest of the area and in E-W direction at the central part of the area, and the both lines seem to cross at the center of the area together. While, the southern zone is composed of two small zones, namely, the zone extending toward the south beyond the area, and the zone distributed at the western edge of the area. The former zone seems to reflect the boundary between granite and phillite in NNW-SSE direction, which may correspond to fault structure. However, the latter zone seems to represent only the outer fringe of the low resistivity zone, the center of which may be located at the south beyond the area, hence it is very difficult to discuss the causative body.

2) -100 m G.L. (Figure II-2-15(2))

Low resistivity zones are more widely distributed than those at -50 m G.L.

The three high resistivity zones are distributed at the western, northern and eastern parts of the survey area. Among these zones, the western zone shows a similar distribution pattern as

that on the -50 m G.L., suggesting that the high resistivity rock extends up to this level, i.e. -100 m G.L. The northern zones show a small-scale distribution pattern in N-S direction at the central part of each of the Lines-A and -B. And the southern zone is composed of the five independent zones in small scale, and the difference of the distribution patterns of between -50 m G.L. and -100 m G.L. suggests the abrupt variation of the structure between both levels.

The low resistivity zones increase those distribution area with the decrease of areas of the high zones, and are widely distributed at the southwestern and central parts of the survey area. The southwestern zone is distributed in NNW-SSE direction at the western part of the zone, and extends to the central zone at the southern end of the zone. While, the central large-scale zone is composed of the N-S trending zones and the E-W trending zones, and seems to reflect homogeneous low resistivity formation (phyllite including graphite) distributed widely, and fracture/shear zones accompanied by the geotectonic lines.

3) -200 m G.L. (Figure II-2-15(3))

The large-scale low resistivity zone is distributed at the whole survey area, and the high resistivity zones are observed in small scale at the eastern and western edges of the survey area.

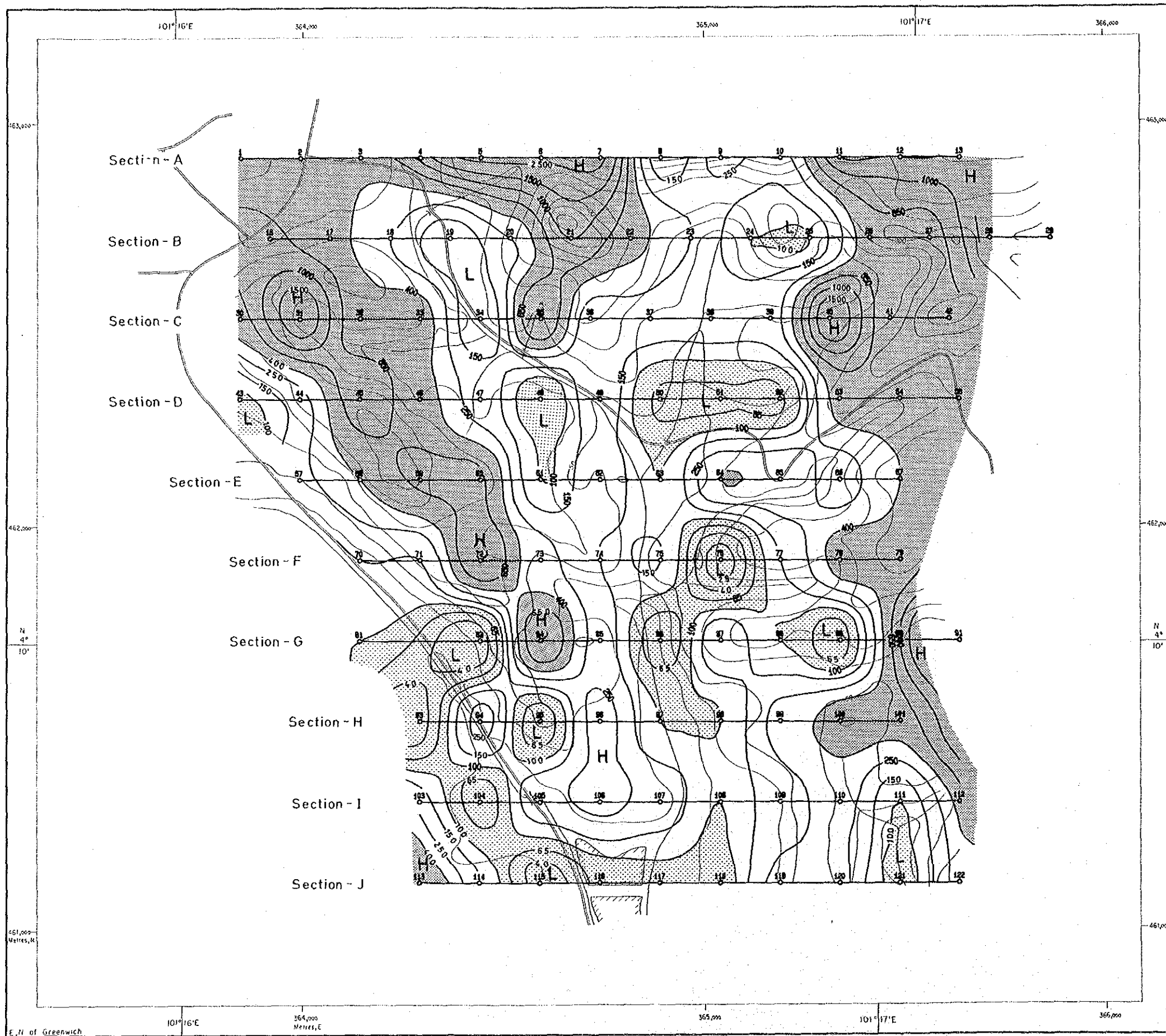
Among the two high resistivity zones, the western zone is composed of three small zones trending in NNW-SSE direction, and the eastern zone is distributed locally at the northeastern and southeastern edges of the area. The former zone is an extension of high-resistivity rock observed on the plan map of each level of -50 m G.L. and -100 m G.L., and this distribution suggests that high-resistivity rock extends toward the depth. And the latter zone seems also to be an extension of high-resistivity rock from the upper levels, but the zone in this level is smaller than that in the upper level.

2-3-2 Discussion on the Results of Geophysical Survey

In the following sections, the results of the CSAMT survey are summarized and the discussions about the survey results are described:

(1) Resistivity Plan Distribution

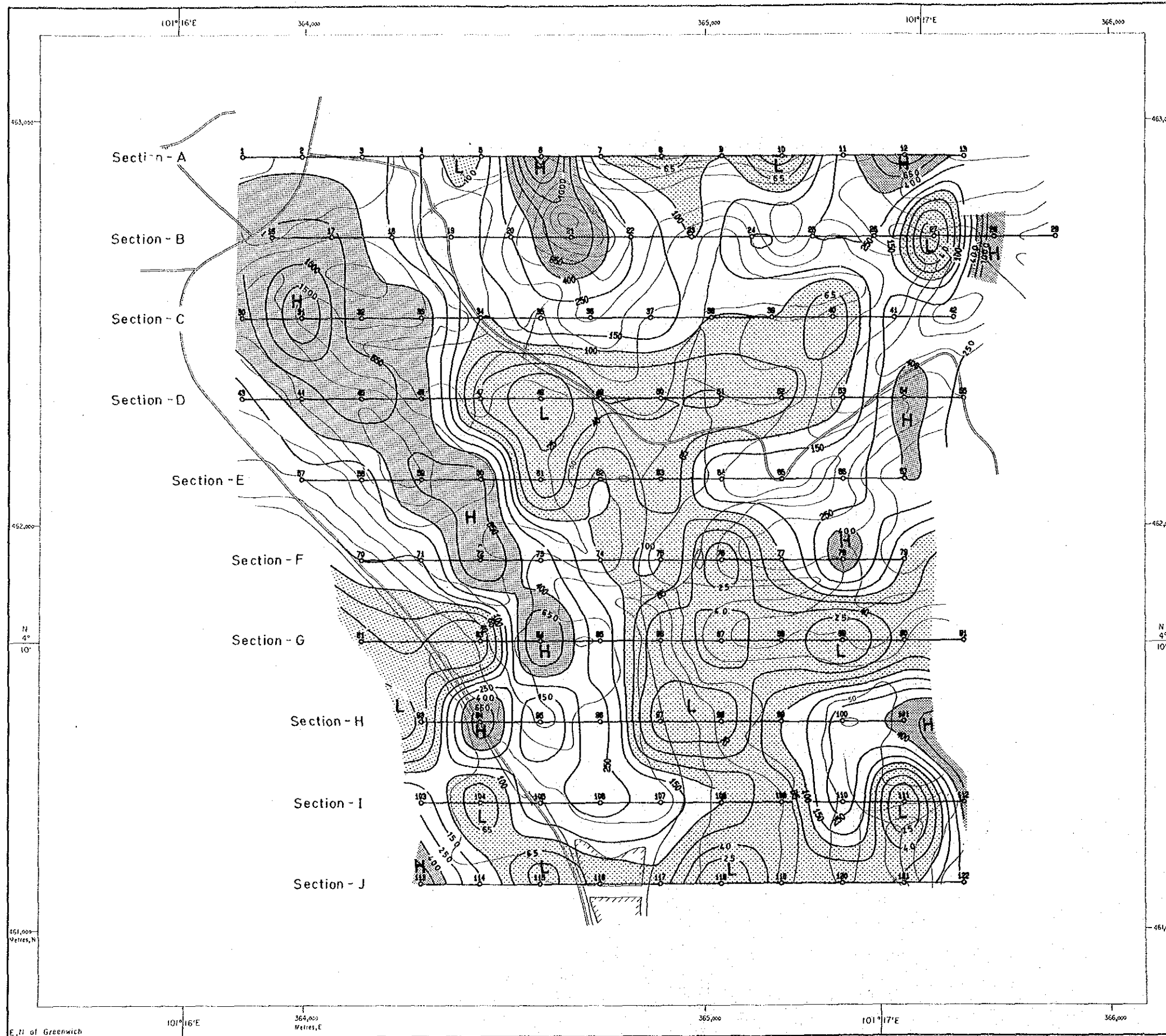
The resistivities in the survey area are classified into three classes, high, medium and low resistivities. Resistivity of each class is of more than 400 Ω -m, of 100 Ω -m through 400 Ω -m, and of less than 100 Ω -m, respectively. And the resistivity zone corresponding to each resistivity class is called high, medium and low resistivity zones, respectively.



LEGEND

- Station and No.
- Resistivity Contour
(Unit: ohm-m)
- $\rho < 100 \text{ ohm-m}$
- $400 \text{ ohm-m} \leq \rho$
- * ρ : Resistivity

Fig. II-2-15 (I) Resistivity Structural Map (-50m G.L.)



LEGEND

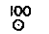



-  Station and No.
-  Resistivity Contour (Unit: ohm-m)
-  $\rho < 100 \text{ ohm-m}$
-  $400 \text{ ohm-m} \leq \rho$
- * ρ : Resistivity

Fig. II-2-15(2) Resistivity Structural Map (-100m G.L.)

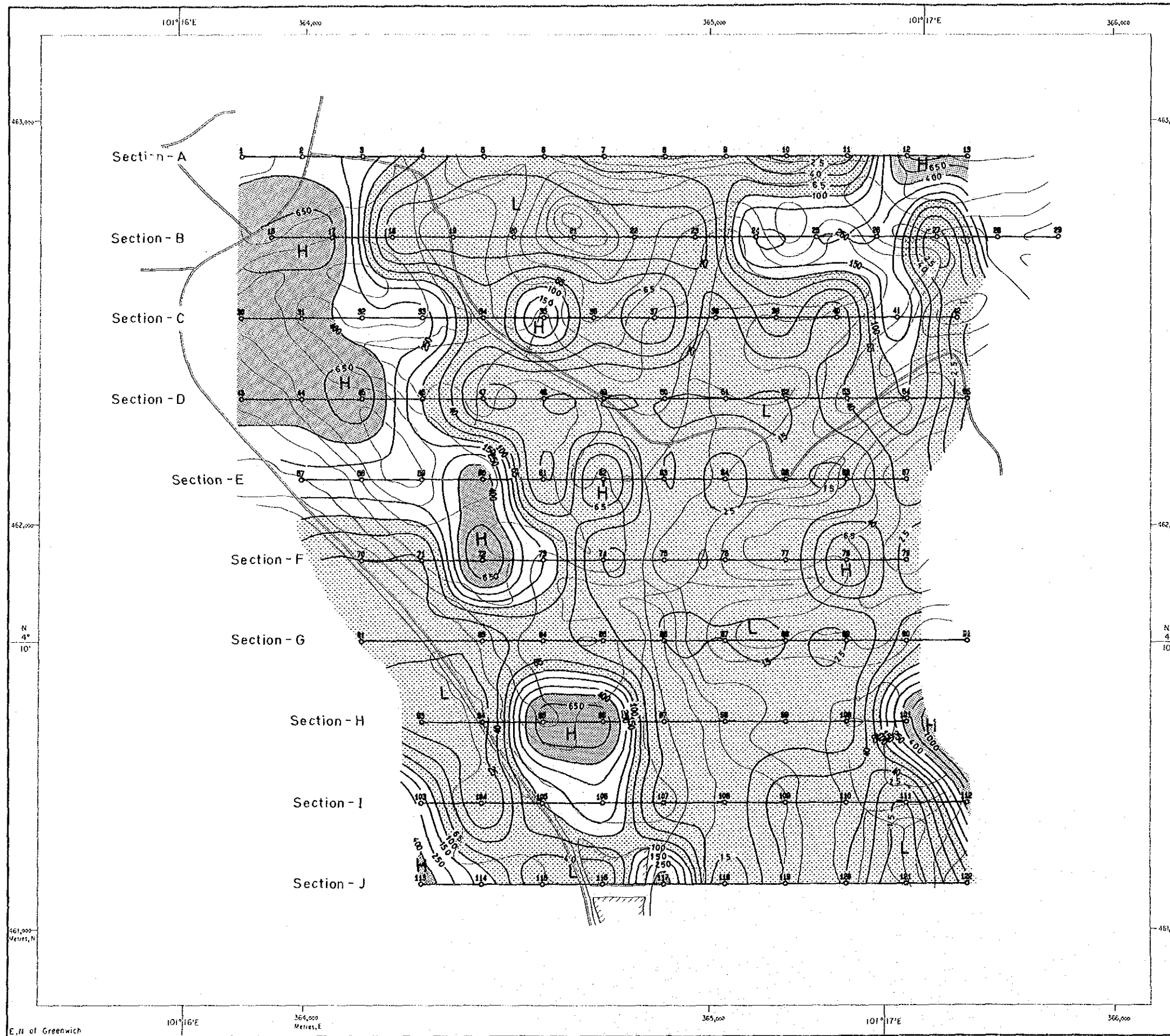


Fig. II-2-15(3) Resistivity Structural Map (-200m G.L.)

1) High Resistivity Zone

High resistivity zones are observed at the western part, at the southwestern edge and at the eastern part of the survey area.

The western zone is distributed in a direction of NNW–SSE, and shows a length of 1,600 m and a width of 300 m to 400 m in the north and about 100 m in the south. This zone extends towards the depths.

Each of the zones at the southwestern edge and at the eastern part is a part of high resistivity zones distributed beyond the survey area.

Each of these three zones shows an extension towards the depth, but the width and resistivity values in each zone vary notably.

2) Medium Resistivity Zone

The medium resistivity zones are observed at the east of the NNW–SSE trending high resistivity zone, and at the shallower part than –200 m G.L. at the eastern part of the survey area. Each of those seems not to extend toward the depth and show a sheet-like distribution. The former zone shows constant resistivity, but in the latter zone there are found high resistivities locally.

3) Low Resistivity Zone

At the depth of shallower than –300 m G.L., the low resistivity zone, distributed at the central part of the survey area, shows a “Y” shape distribution pattern which is similar to that of creeks, and the small-scale low resistivity zones trending in NNW–SSE and N–S directions are observed in the province of this “Y” shape zone.

And, at the depth of deeper than –300 m G.L., the above “Y” shape low zone forms a large-scale low resistivity zone by absorbing the surrounding small-scale zones. The variation of resistivities in this large-scale zone is little.

And another low resistivity zone is distributed at the west of the NNW–SSE trending high resistivity zone observed at the western part of the survey area. This low zone is found in small scale below the high resistivity zone at the north of Line–D, but at the south of Line–D this zone increases its distribution area toward the south.

(2) Resistivity Structure

There are found many resistivity discontinuities running in various directions in the survey area, and the resistivity structure shows a distribution controlled by these resistivity discontinuities.

- 1) The resistivity structure in the survey area shows a vertical structure at the western part, and a horizontal structure at the eastern part.
- 2) The vertical resistivity structure is observed in the high resistivity zone in particular, showing a trend of NNW–SSE direction, and extends towards the depth.
- 3) The horizontal resistivity structure is found in the whole eastern part of the survey area, and shows a two-layer structure of shallow-high and deeper-low.
- 4) There are presumed a lot of resistivity discontinuities, which cluster the resistivity structure into blocks.
- 5) These resistivity discontinuities trending in NNW–SSE and NNE–SSW directions are presominantly distributed. Those of NNW–SSE direction are observed at the western part, and those of NNE–SSW direction at the eastern part.
- 6) Medium resistivity layer shows the thickness of less than 100 m at the central part, and becomes thicker toward the east.

(3) Relation Between Resistivity Zones and Geology (Fig. II-1-16)

The geology in the survey area consists of granite at the western edge, metasandstone at the western part, and phyllite at the central-eastern part. And the geological structure strikes NNW–SSE direction and dips sharply toward the west. Each of resistivity zones seems to reflect well the characteristics of the formations, as mentioned below.

- 1) High resistivity zones
 - a) The zone distributed in a NNW–SSE direction at the western part seems to correspond to granite.
 - b) The zone at the southwestern edge seems to represent a part of high resistivity rock, corresponding to granite.
 - c) The zone at the eastern part is distributed locally in the medium resistivity zone and is observed in a distribution area of phyllite. Hence, this zone may correspond to meta-sandstone existing in lense-shape in phyllite.
- 2) Medium resistivity zone
 - a) The zones are observed in a distribution area of phyllite. However, phyllite seems to be of low resistivity as described later, it is thought that fractures in phyllite are developed notably at the shallower part.
 - b) The zone shows a constant resistivity in the whole area, except for the eastern part where metasandstone existed in phyllite, so that phyllite at the shallower part seems to be in same condition in the whole area.

3) Low resistivity zone

- a) Low resistivity zones are observed in phyllite distribution area. In this distribution area, phyllite includes graphite so that phyllite in this area is thought to show lower resistivity than general phyllite.
- b) A large-scale low resistivity zone at the central-eastern part may reflect phyllite including graphite and developed resistivity discontinuities also.

4) Resistivity discontinuities

- a) The resistivity discontinuities trending in NNW–SSE, NW–SE, NE–SW and N–S directions are observed, and cross together at the center of the area.
- b) The NNW–SSE trending ones are observed at the both sides of high resistivity zones at the western part and at the central-northern part. The one at the west of high resistivity zone may reflect the fault structure being the boundary between granite and metasandstone. While, the one at the east of the zone is located at the boundary between high and low resistivity zones, and may reflect either the fault structure or the weak part of the formation.
- c) The ones trending in NW–SE, NE–SW and N–S directions may reflect the weak parts of the formation, and show similar directions as those of creeks at the central part.

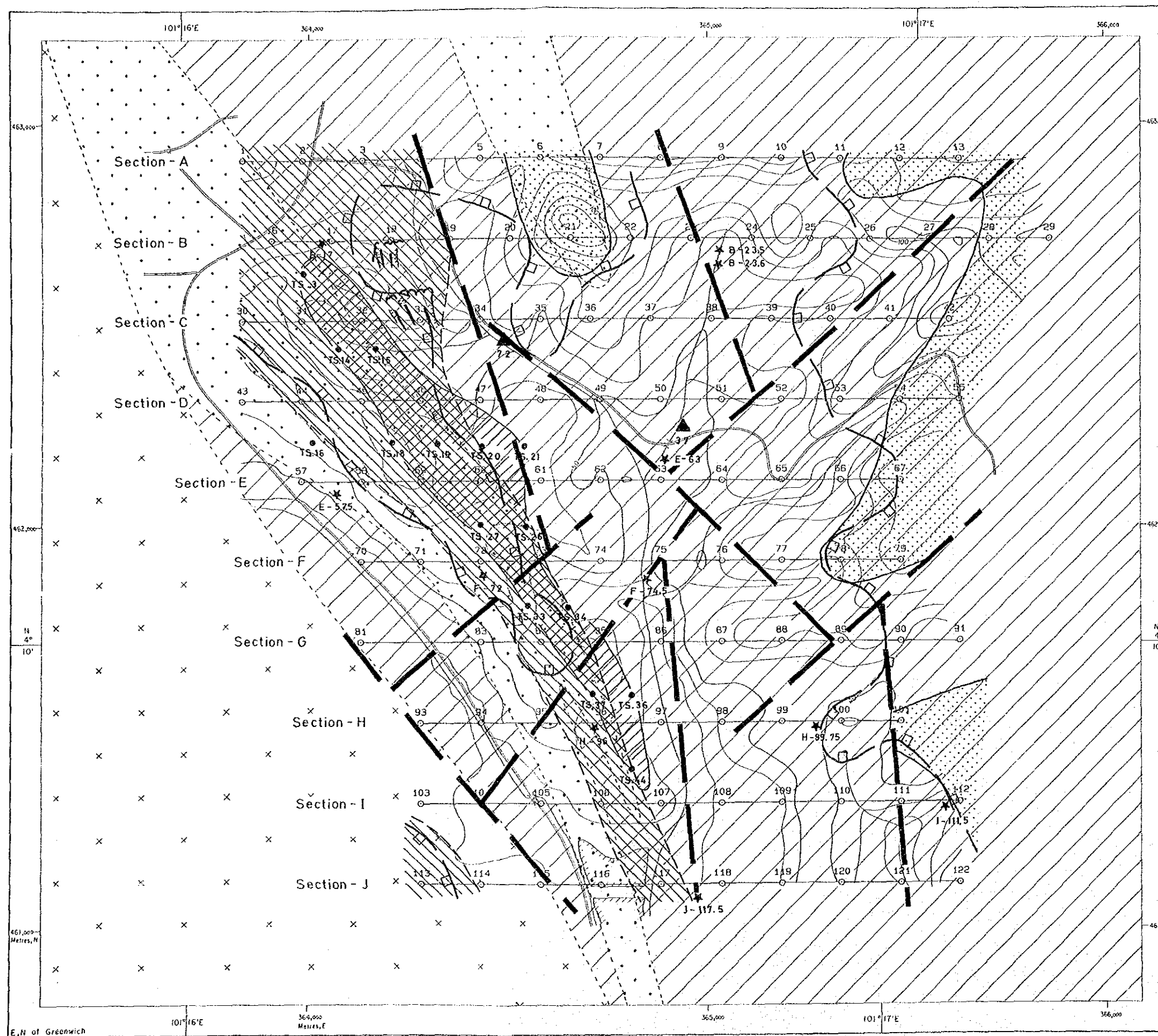
Therefore, the results of the CSAMT survey are summarized as follows:

- (1) High resistivity zones, detected at the western and eastern parts of the area, seems to reflect metasandstone with rich quartz.
- (2) Quartz veins, seemed to be distributed in the area, may be very thin and very short, and occur scarcely.
- (3) Low resistivity zone, distributed at the whole central-eastern part of the area, may be caused by both phyllite including graphite and fracture zones developed at the weak part of the formation.

2-4 Discussion

Summing up the results of geological and geochemical surveys, the Area A seems to have high potential for gold resources and, therefore, it is important to carry out exploration mainly for gold.

The geochemical survey in this phase disclosed a large-scaled gold anomaly zone with an area of (2–4) km x 22 km, lying parallel to the Tapah–Bidor–Sungkai highway. It is reportedly known that the Quaternary deposits on the west of the Tapah–Bidor highway produced placer



LEGEND

- 100 Station and No.
- Resistivity Discontinuity Line
- Sampling Point and No. (for Electrical Property)
B-17
- 2-D Model Analysis**
- High Resistivity Layer/Rock (Depth > 300 m G.L.)
- High Resistivity Layer/Rock (Depth < 300 m G.L.)
- High Resistivity Zone more than 400ohm-m (from -50m G.L. Resistivity Structural Map)
- Geochemical Anomaly**
- TS.14 Station Where Au Flakes are found in Soil
- 72 Au Value (ppm) in Stream Sediments
- Au Anomaly Zone in Soil
- Geology**
- Changkat Rembian Granite
- Metasandstone
- Phyllite
- Bukit Mas old Workings

Scale 1:10,000

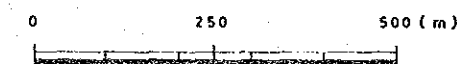
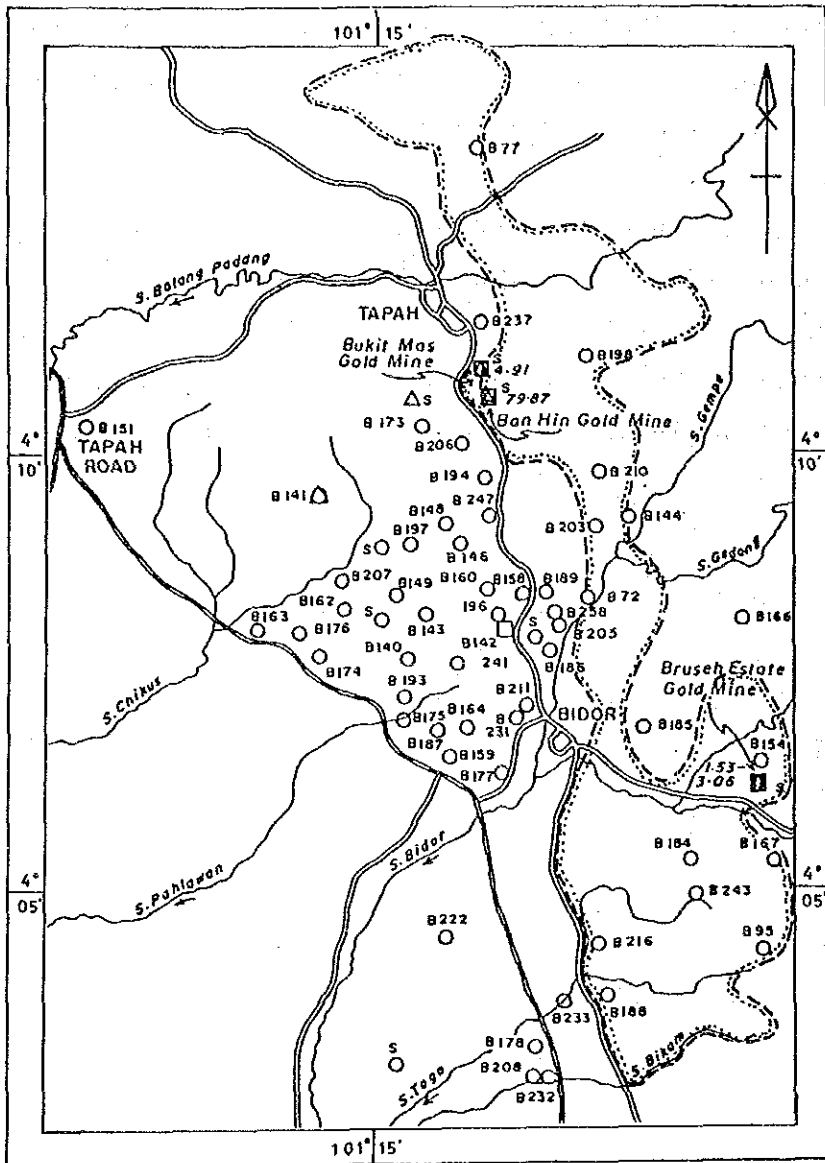


Fig. II-2-16 Interpretation Map

gold. As shown in Fig. II-2-17, the gold anomaly zone seems to be the source of placer gold.

The gold anomaly zone includes the Bukit Mas gold mine area but gold contents per unit volume of the area on the north of the S. Batang Padang, are much higher than those of the Bukit Mas area.

Besides, it is regarded from the CSAMT survey results that the Bukit Mas gold deposit is of a small scale because a favourable resistivity structure for mineralization was not detected. But the gold anomalies found by GSM soil sampling indicate gold mineralization in the sandstone of a upper horizon, therefore, it is necessary to explore this mineralization. However, an exploration programme for the Bukit Mas area should decide based on the exploration results not only in the Bukit Mas area but also in the whole anomaly zone.



Kilometres 2 1 0 2 4 6 Kilometres

LEGEND

△	- Primary gold occurrence		Gold geochemical anomaly zone (MMAJ-GSM)
○	- Placer gold occurrence		
□	- Former gold mine		
B 222	- Geological Survey archive serial number		
4.91	- Gold value in ppm.		
S	- Sampled by GSM.		

(After Vijayan, 1985)

Fig. II-2-17 Gold Occurrences in Tapah-Bidor Area

Chapter 3 Area B

3-1 Study on the existing data

The investigation of Quaternary formations, extending from the west of the Area A, has been carried out by GSM.

The investigation area which includes the Changkat John sheet (which was initially proposed as the Area B) is still under compiling process. The data on the Taluk Intan sheet, where the GSM's alternative area is located, were compiled into a report by Loh C.H. (1987). He studied the Teluk Intan sheet together with the west of Tapah sheet. However, the Quaternary formations in the Tapah sheet has not yet been drilled by GSM.

The existing data can be summarized as follows.

(1) Teruk Intan Area

Due to the lack of surface exposures, the nature of the Quaternary formations were investigated through 175 shallow boreholes and 22 deep boreholes.

1) Geology

The Bedrock consists of late Paleozoic sedimentary rocks which are intruded by Triassic granites. They are unconformably covered by the Simpang Formation of Pleistocene and the Gula and Beruas Formations of Holocene.

The Simpang Formation is composed of terrestrial clay, silt, sand and gravel with subordinate amount of peat, and is believed to be made up largely of alluvial fan-braided river deposits. The thickness of the formation is 40-60 m.

The Gula Formation is composed of marine clay, silt and sand with subordinate amount of gravel. It includes a small amount of shell fragments. Fossil evidence suggests a shallow marine to estuarine environment of deposition for the Gula Formation. The Formation is 0 m - 40 m thick, covering the Simpang Formation conformably.

The Beruas Formation, the youngest formation in the area, is of a terrestrial (fluvatile) type, consisting mainly of clay, silt, sand, gravel and peat. This formation is contemporaneous with and in parts younger than the Gula Formation. The thickness of the formation is about 15 m.

2) Heavy Minerals

The heavy minerals identified in the formations are ilmenite, monazite zircon, rutile,

tourmaline, topaz, pyrite, magnetite, siderite and cassiterite. Regarding cassiterite, the following trends were pointed out by Loh, C.H. (1987).

(a) Placer tin deposits occur only in the Simpang Formation.

The Beruas Formation and the Gula Formation do not contain significant amounts of tin.

(b) In the Labu Kubung area, placer tin deposits are confined to sand and gravel layers near or on the bedrock and cannot be expected on a shallow level. The distribution of cassiterite in the area indicate the source of tin to be the Tanjong Tualang region in the north and that rich tin placers are not likely to be found on the west of the Labu Kubung area and on the south of the Sungkai Manik area.

(c) In the Seberang Perak, placer tin deposits are restricted to sand and gravel layers found within 20–30 m below ground surface. Deep seated deposits near the bedrock are hardly found. In the Bandar area, a drill hole 64Qd03 penetrated a 6 metre thick layer bearing 0.18–0.32 kg/m³ of cassiterite, so that shallow placer tin deposits are expected to be here.

(2) Changkat Jong Area

More than 30 shallow and 20 deep boreholes were drilled in the paddy field in order to clarify the nature of Quaternary formation.

1) Geology

The Bedrock, composed of late Paleozoic formations and Triassic granites, are overlain (as in the Teruk Intan Area) by the Simpang Formation of Pleistocene and the Gula and Beruas Formations of Holocene.

The Simpang Formation is composed of clay, sand, gravel and peat and is a little rich in gravel compared with that in the Teluk Intan Area. The thickness of the formation is 10–40 m.

The Gula Formation is contemporaneous with the Beruas Formation, the former of which mainly consists of humic clay but the latter, gravel with humic clay at the top.

2) Heavy Minerals

The heavy minerals in each formation are ilmenite, zircon, monazite, xenotime, rutile, tourmaline, topaz, pyrite and others. However, little cassiterites occur.

Fig. II-3-1 and Fig. II-3-2 shows the location map of boreholes and geological sections with SnO₂ contents.

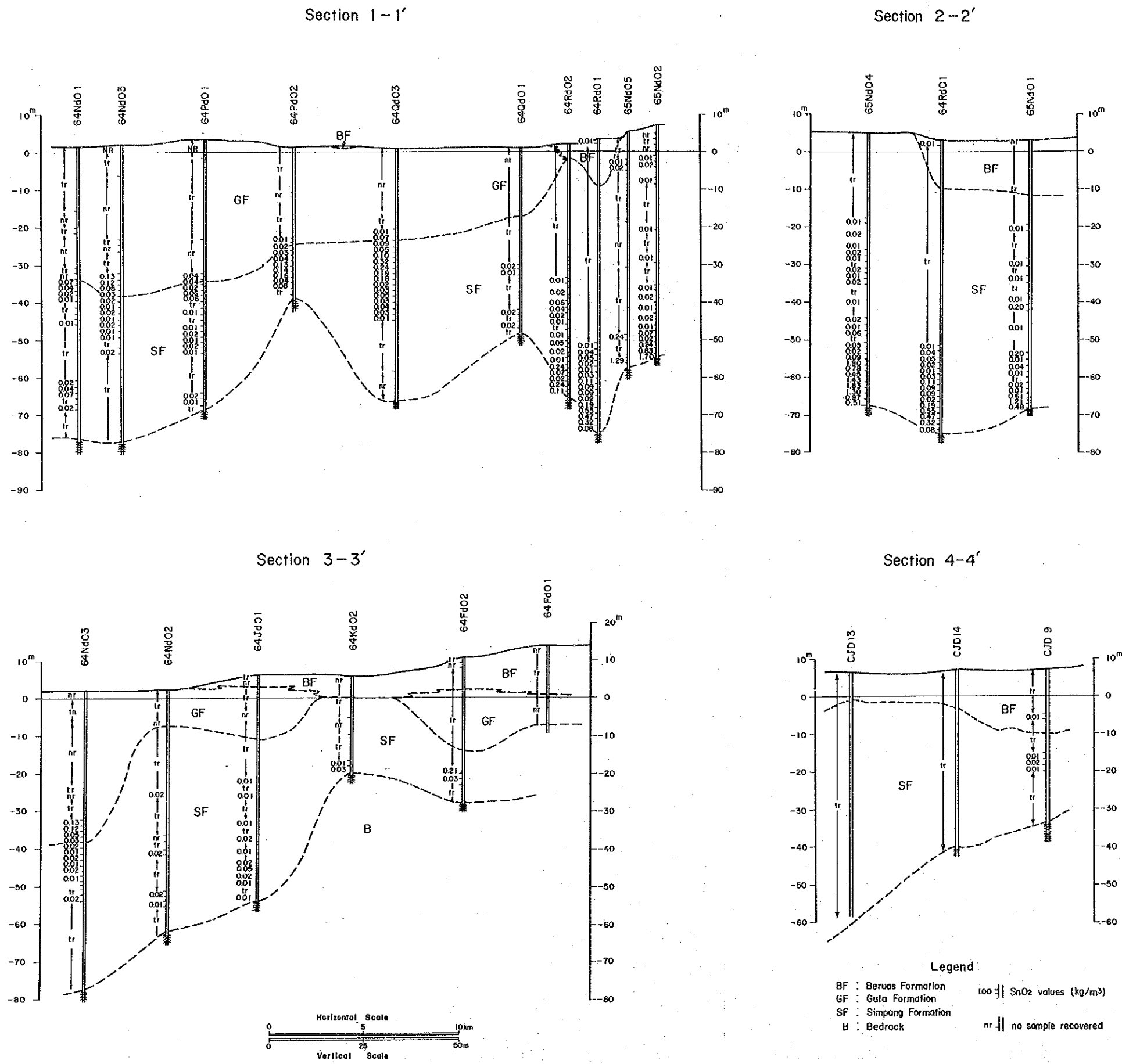


Fig. II-3-2 Quaternary Geological Sections in the Teluk Intan Area

3-2 Discussion

Eight deeper boreholes in the Changkat Jong area indicate that depth of the bedrock from the surface ranges from 15 to 70 m and ballclay of a good quality is intercalated. However, very recent GSM studies disclosed the followings.

- (1) As indicated by three boreholes (CJD9, CJD13 and CJD14), the composition of heavy minerals are almost same.
- (2) The average amount of heavy minerals is 0.3 kg/m^3 .
- (3) The constituent minerals are 65-80% ilmenite, 9% zircon, <2% monazite, 0.5-2.0% xenotime. Few the ore minerals are included.

Judging from the location, the alluvium deposits in the changkat Jong area seem to originate from the basins of S. Sungkai and S. Selim (that is, the Tanjong Malim area). Therefore, based on the facts that the geochemical results in this phase do not indicate a high potential for heavy mineral resources in the Tanjong Malim area and that the results of deeper boreholes are not attractive, it can be concluded that tin and other heavy minerals are not promising in the Changkat Jong area.

By contrast, at the Labu Kubung in the Teluk Intan area, 6 deeper boreholes intersected good tin concentration with a 1.5 to 6.0 m width, lying on or near the bedrock which is 80 m deep from the surface. The SnO_2 contents vary from 0.24 to 1.29 kg/m^3 .

The six boreholes are in an area of 3 km x 8 km and some extension in tin concentration toward northeast can be expected. As the tin concentration is considered to be much affected by the bedrock profile, it is needed to investigate the bedrock relief before designing a drilling programme.

Another concentration of 6.0 m width and 0.25 kg/m^3 lies between the surface and the bedrock at Bandar (64 Qd 03) on the west of S. Perak. A grid drilling would be the most recommendable method to explore the extension of this concentration.

Chapter 4 Area C

4-1 Geology

The Area C is mainly composed of Paleozoic mica schist–phyllite which are intruded by the Main Range granite and Quaternary sediments. A geological map and a generalized stratigraphic section in this area are shown in Fig. II-4-1 and Fig. II-4-2.

4-1-1 Stratigraphy

(1) Paleozoic

Distribution : The Paleozoic is distributed in the northern area.

Rock Facies : The rocks are composed of mica–quartz–schist, chert, mica schist–phyllite and chlorite–rich mica schist in an ascending order.

Mica–quartz–schist is distributed near the granite. It has a clear schistosity and a banding structure, consisting of quartz and mica.

Chert thinly overlies the mica–quartz–schist. It is grey in colour and very hard. It has poor schistosity.

Mica schist – phyllite is dark grey to black in colour, well schistose and rich in fissility. It is commonly accompanied with segregation vein with 1 – 10 cm in width. Some veins contain pyrite.

Chlorite–rich mica schist is observed at the exposure as green coloured mica schist.

Under microscope is also observed, quartz sericite–muscovite and fairly good chlorite.

Age of Deposition : It is considered to be lower Paleozoic.

(2) Quaternary

Recent sediments are distributed along rivers. However they are not mappable due to limited exposures.

4-1-2 Intrusive Rocks

The intrusive rocks in the area is the Main Range granites.

(1) Main Range granite

Distribution : It occupies the area from the central to the southern partion.

Rock Facies : The Main Range granite can be lithologically divided into porphyritic and equigranular, leucocratic granite, aplite vein, quartz vein and pegmatite vein occur in the

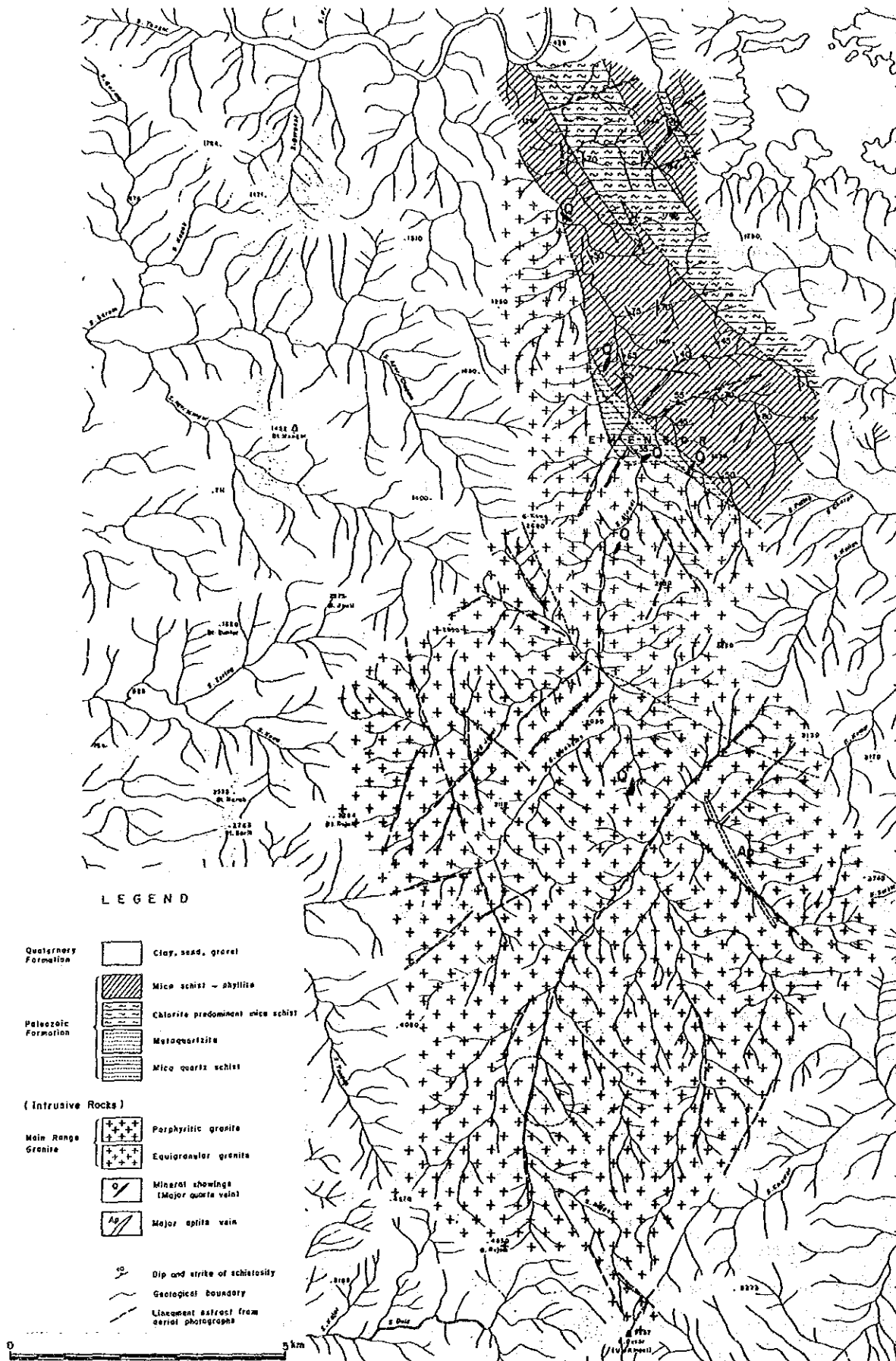


Fig. II-4-1 Geological Map and Distribution Map of Mineral Showings of the Area C

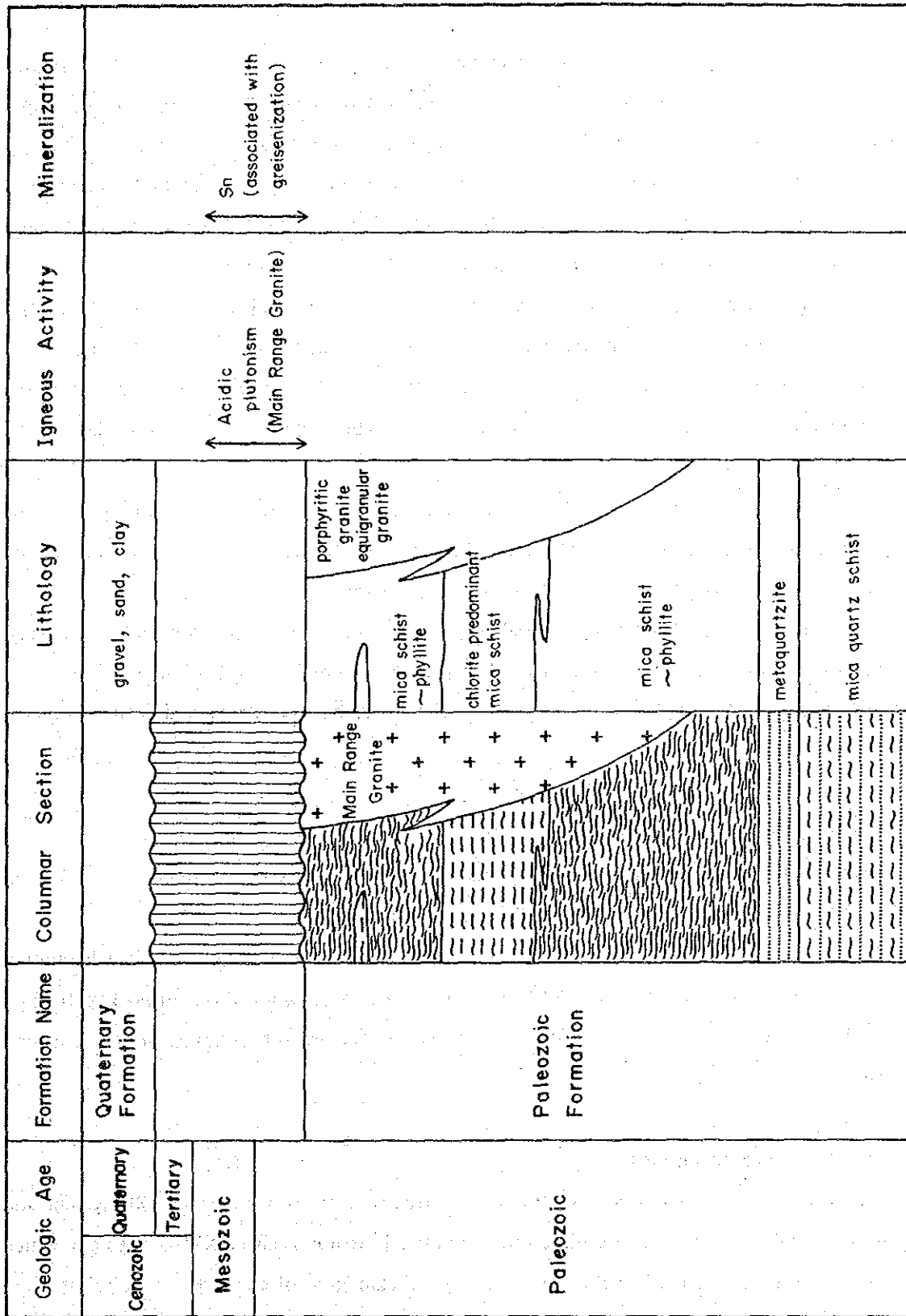


Fig. II-4-2 Stratigraphic Section of the Area C

porphyritic granite.

The porphyritic granite, which occupies the southern half of the area, is characterized by megacrystals of K-feldspar with a 2 – 5 cm length. Under microscope, main component minerals are quartz > K-feldspar · plagioclase > biotite > muscovite. K-feldspar consists of orthoclase and microcline. The ratio of both minerals is considerably variable.

A perthite texture and carlsbad twin are well developed in K-feldspar. Plagioclase and biotite are altered strongly to sericite/kaoline and chlorite respectively.

The equigranular granite composes the contact zone with Paleozoic rocks in the central part of the area. It is also distributed in a small scale in the upper reaches of S. Ringat. It is coarse-grained and its main components are same as those of the porphyritic one. Near the contact with the Paleozoic rockes, xenoliths (mica schist) with 2 – 5 cm in size are characteristically included.

Leucocratic granite occurs locally in the porphyritic granite near the contact with the equigranular granite. It is finer-grained than porphyritic and equigranular, being mainly composed of quartz, K-feldspar (orthoclase and microcline) and muscovite and/or biotite.

Most of veins of aplite quartz and pegmatite do not exceed 30 cm in width. However, the aplite vein in the east central area is 5 m in width and more than 1.5 km in length.

Age of Intrusion : As mentioned in Chapter 2, the intrusion age is regarded to be Permian–Triassic.

(2) Chemical Composition of Granite

Seven pieces of granite samples from this area were analyzed. The results are shown in Table II–2–1 together with the results of those from the Area A.

As clearly shown in Fig. II–2–3 (Norm Q–An–(Or + Ab) Diagram), these 7 samples fall in the same field as the Area A, indicating a homogeneous composition. From Fig. II–2–4 ($\text{Fe}_2\text{O}_3/\text{FeO}$ Diagram) it can be seen that they belong to the ilmenite series except for leucocratic granite.

4–1–3 Geological Structures

The Paleozoic formation has a monoclinic structure, striking in a NW–SE system and dipping 40 – 80° toward NE. The direction of granite intrusion is also a NW–SE system, which prevails over the area. On the contrary, joints and lineaments interpreted from airphotos are oblique to the above direction. Especially, the lineaments which are developed in the western granite, tend to meet at a right angles (NE–SW system).